

1 We would like to thank the reviewers for their comments which have improved the manuscript. Specific
2 comments from the reviewers are given in bold below, followed by our responses in plain text.

3
4 **Referee #1**

5
6 **Stone et al. presents a study on the influence of tropospheric halogens on OH and HO₂. The study is based on**
7 **observations from the Cape Verde Atmospheric Observatory, a chemistry box model, and a global chemical**
8 **transport model. Overall, the paper is well written and well suited for ACP. I recommend it being accepted**
9 **following minor revision. I list specific comments and questions below:**

10
11 **1) Line 49: Le Breton et al (2017, doi: 10.1016/j.atmosenv.2017.02.003) have also presented measurements of**
12 **BrO in the MBL, consider including a citation.**

13
14 We have included the citation.

15
16 **2) Line 224: What are the processes behind "Physical loss", is it deposition? If so, I suggest you state this**
17 **explicitly. Is a lifetime of 24 hour reasonable?**

18
19 The physical losses incorporate losses such as wet and dry deposition and diffusion out of the box for any model
20 generated species with a sufficiently long lifetime. In our previous work (Stone et al., 2010; Stone et al., 2014)
21 we investigated the sensitivity to the deposition rate, with results indicating that variation of the deposition
22 lifetime between 1 hour and 5 days results in little change to the modelled concentrations of OH and HO₂. We
23 have added the following details to the manuscript for clarification:

24
25 *Deposition processes, including dry deposition and wet deposition, and diffusion are represented in the model by*
26 *a first-order loss process, with the first-order rate coefficient equivalent to a lifetime of approximately 24 hours.*
27 *As discussed by Stone et al. (2010), variation of the deposition lifetime between 1 hour and 5 days results in*
28 *limited changes to the modelled concentrations of OH and HO₂.*

29
30 **3) Line 244 to 253: The assumption of constant BrO and IO between 9:30 and 18:30 seems overly crude. As**
31 **can be seen in Figure 3 of Read et al. (reference given in manuscript), it takes approximately 6 hours for BrO**
32 **and IO to raise from 0 to max. How would the results of the box model study change is more realistic**
33 **assumptions about the diurnal cycle of BrO and IO are used?**

34
35 The peak daytime concentrations of BrO and IO are typically reached between 9 am and 10 am, with increases
36 from zero occurring from approximately 6 am, as shown in Figure 3 of Read et al. The discussion in the
37 manuscript is unaffected by the early morning concentrations of BrO and IO owing to the focus on the midday
38 (11 am to 1 pm) concentrations of OH and HO₂, and the HO₂:OH ratio, which are influenced on short timescales.
39 The data presented in Figures 1-3 are potentially affected by the assumption of zero concentrations of BrO and
40 IO before 9:30 am, and we have performed simulations in which concentrations of BrO and IO are set to increase
41 from 6 am until 10 am, at which point the constant concentrations are reached, using the data shown in Figure 3
42 of Read et al. However, the low concentrations of BrO and IO during this period, and the relatively few data
43 points for OH and HO₂ during these times (there were no measurements of OH or HO₂ at these times of day

44 during SOS2, as shown in Figures 1 and 3), the data presented in the manuscript are not significantly affected.
45 This is shown in the figure below (Figure S6), combined with the response to referee 2. We propose to combine
46 this figure and to provide the details in the supplementary information to the manuscript.
47

48 **4) Line 288 to 291: Please specify the additional bromine reactions that were added to the Parella mechanism.**
49

50 We apologise for the confusion here. The additional bromine reactions are those described by Parella et al. (i.e.
51 in addition to the standard mechanism which does not include any halogen chemistry). We have removed the
52 reference to “additional” in order to clarify this:
53

54 *Emission rates and bromine chemistry included in the model are described in detail by Parella et al. (2012), with*
55 *the bromine chemistry scheme described by 19 bimolecular reactions, 2 three-body reactions and 2*
56 *heterogeneous reactions using rate coefficients, heterogeneous reaction coefficients and photolysis cross-sections*
57 *recommended by Sander et al. (2011).*
58

59 **5) Line 477-481: Consider extending the discussion of sea-salt debromination. Schmidt et al (reference given**
60 **in manuscript) presented two simulations: one without sea salt debromination and one including it. The**
61 **simulation that included sea salt debromination led to levels of BrO that appeared biased high compared to**
62 **satellite observations, but reproduce the levels observed in the mid Atlantic MBL (see Figure S8 of Schmidt et**
63 **al.). How would the result of the global model change if sea salt debromination was included?**
64

65 We have expanded the discussion of this in the manuscript to include the following details:
66

67 *The global model simulations reported here predict average mixing ratios of ~0.5 ppt for BrO and ~1 ppt for IO*
68 *during SOS, and thus underpredict BrO but perform well for IO. The underprediction of BrO at Cape Verde*
69 *results from recent model updates which exclude emissions of bromine species from sea-salt debromination*
70 *(Schmidt et al., 2016) in order to provide improved agreement with observations of BrO made by the GOME-2*
71 *satellite (Theys et al., 2011) and in the free troposphere and the tropical Eastern Pacific MBL (Gomez Martin et*
72 *al., 2013; Volkamer et al., 2015; Wang et al., 2015). If sea-salt debromination were included, daytime mixing*
73 *ratios of BrO at Cape Verde would be approximately 2 ppt, as shown by Parella et al. (2012) and Schmidt et al.*
74 *(2016), and thus in closer agreement to the observations. Increased modelled concentrations of BrO at Cape*
75 *Verde resulting from inclusion of sea-salt debromination would have a greater effect on OH and HO₂, leading to*
76 *more significant decreases in OH and HO₂ when bromine chemistry is included without iodine chemistry, with*
77 *the larger decrease in OH potentially off-setting the increase in OH observed when bromine and iodine chemistry*
78 *are combined. However, the current model simulations do not consider the coupling between bromine and sulfur*
79 *chemistry, which may represent a significant sink for reactive bromine species in the troposphere and balance*
80 *sources from sea-salt debromination (Chen et al., 2017). These results thus demonstrate the need for further*
81 *investigation and constraint of sources and emission rates of bromine species, and of the coupling between sulfur*
82 *chemistry and reactive bromine species. We now discuss the global impacts of halogen chemistry.*
83
84
85

86 *Also, consider commenting on the resent study by Chen et al (2017, doi: 10.1002/2017GL073812) that show*
87 *that sulfur chemistry may provide a missing sink of Bry in the MBL to balance the sea salt debromination*
88 *source.*

89
90 We have now included details of this study in our discussion of sea-salt debromination (see above).

91
92

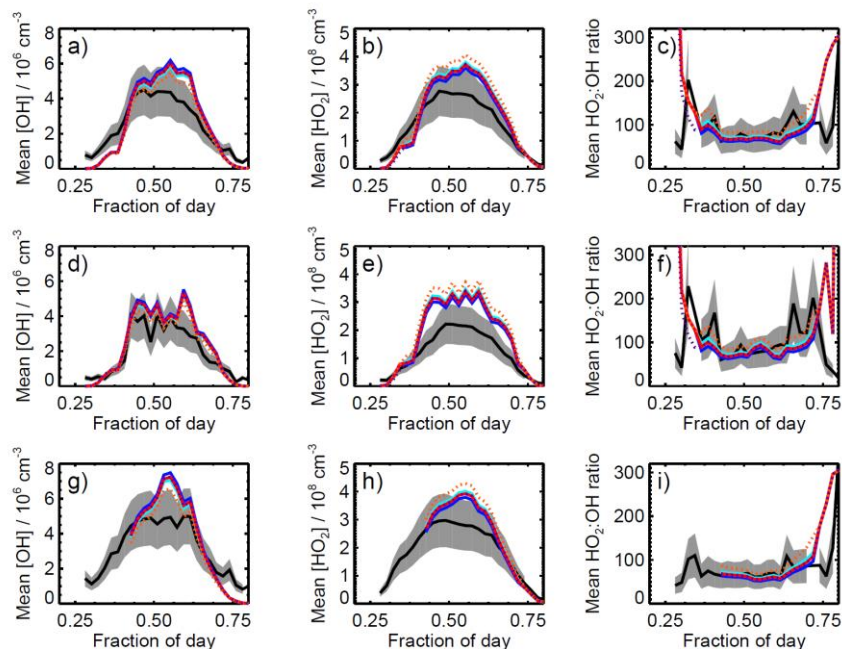
93 **Referee #2**

94
95 *The paper presents an interesting comparison between observations of OH and HO₂ at the Cape Verde*
96 *Observatory and two modelling approaches to evaluate how bromine and iodine chemistry impacts HO_x. The*
97 *results obtained by the two different model setups are discussed and evaluated in the context of the different*
98 *chemical schemes and timescales considered in the two models. I found the paper interesting and well*
99 *structured, presenting results in a clear and complete format and hence I recommend the paper for publication*
100 *in ACP. Please find below two questions and minor comments for consideration by the authors:*

101 *- In page 9, line 244, it is written that the box model is constrained by the mean observed mixing ratio of BrO*
102 *and IO, 2.5 and 1.4 pptv, respectively. What was the peak value of BrO and IO in the model runs?, if the peak*
103 *value used was 2.5 and 1.4, did you run a sensitivity with the XO peak values measured by Read et al., 2008*
104 *and Mahajan et al., 2010?*

105
106 The peak values used in the model simulations were 2.5 ppt BrO and 1.4 ppt IO. We have now performed a
107 sensitivity analysis to these mixing ratios, using the upper and lower limits to the diurnal averages reported by
108 Read et al. (3.5 ppt and 1.5 ppt for BrO and 2.0 ppt and 1.0 ppt for IO). The impacts of these changes on the
109 diurnal profiles for OH and HO₂, and on the HO₂:OH ratio, are shown in the figure below (Figure S6). Given the
110 focus of the manuscript on the different trends between the box and global models, rather than the absolute
111 concentrations of BrO and IO, we propose to include this figure (Figure S6), which also includes sensitivity to
112 early morning concentrations of BrO and IO as suggested by reviewer 1, in the supplementary information to the
113 paper for completeness. We have added a comment in the main text (line 248) to refer to the sensitivity to BrO
114 and IO concentrations (“Sensitivity to these mixing ratios is discussed in the Supplementary Material”) and have
115 added the following details to the Supplementary Material:

116
117 *Observations of BrO and IO at the Cape Verde Atmospheric Observatory show average diurnal mixing ratios of*
118 *2.5 ppt and 1.4 ppt, respectively, which were used as constraints in the box model simulations presented in this*
119 *work. In order to test the sensitivity of OH and HO₂ to these constraints, we have performed simulations in which*
120 *the BrO and IO mixing ratios were constrained to the upper and lower limits of the observed values (3.5 ppt and*
121 *1.5 ppt for BrO and 2.0 ppt and 1.0 ppt for IO, as reported by Read et al. (2008) and Mahajan et al. (2010)). In*
122 *addition, simulations were performed in which mixing ratios of BrO and IO increase from 0600 hours and reach*
123 *the constant values of 2.5 ppt and 1.4 ppt, respectively, as shown by Read et al. (2008). Results from these*
124 *simulations are shown in Figure S6, and indicate that there are only minor differences in the OH and HO₂*
125 *concentrations between simulations performed on constraining to the upper and lower limits of the observed BrO*
126 *and IO concentrations, and that there is little sensitivity of OH or HO₂ to the early morning mixing ratios of BrO*
127 *and IO.*



129
 130 *Figure S6: Impacts of changes to BrO and IO constraints on average diurnal profiles for a) OH during both*
 131 *measurement periods; b) HO₂ during both measurement periods; c) HO₂:OH ratio during both measurement*
 132 *periods; d) OH during SOS1 (Feb-Mar 2009); e) HO₂ during SOS1; f) HO₂:OH during SOS1; g) OH during*
 133 *SOS2 (May-June); h) HO₂ during SOS2; i) HO₂:OH ratio during SOS2. Observed data are shown in black, with*
 134 *grey shading indicating the variability in the observations; model simulations constrained to the average daytime*
 135 *(0930 to 1830 hours) mixing ratios of BrO (2.5 ppt) and IO (1.4 ppt) are shown in red; simulations constrained*
 136 *to the upper limits to the daytime mixing ratios of BrO (3.5 ppt) and IO (2.0 ppt) are shown in dark blue;*
 137 *simulations constrained to the lower limits to the daytime mixing ratios of BrO (1.5 ppt) and IO (1.0 ppt) are*
 138 *shown in light blue; simulations constrained to the average daytime mixing ratios of BrO (2.5 ppt) and IO (1.4*
 139 *ppt) and including increases in the mixing ratios from 0600 hours are shown by the dashed purple lines;*
 140 *simulations with no halogens are shown by the dashed orange lines.*

141
 142 **- One thing that I miss in this paper is the how halogen-driven changes in NO_x affect HO_x?. There is not**
 143 **mention to this aspect and from previous modelling studies it is expected to have a bearing on HO_x. I would**
 144 **suggest the authors to mention whether they have explored this coupling and perhaps add some additional**
 145 **results to the revised manuscript.**

146
 147 While we do not explicitly discuss the impacts of halogen-driven changes in NO_x on HO_x, this is included in the
 148 model simulations and there are some details in the discussion of the radical budgets and in Figures 4-6 which
 149 show how the role of NO_x chemistry in controlling radical budgets changes on inclusion of halogen chemistry.
 150 We propose to include the following details to discuss these impacts more thoroughly:

151 *The change in the relative importance of HO₂ + NO on inclusion of halogens in the model results from both the*
152 *increase in the total HO₂ sink, owing to the additional losses through HO₂ + BrO and HO₂ + IO, and the shift in*
153 *NO_x partitioning owing to the reactions Br + NO → Br + NO₂ and IO + NO → I + NO₂. The reactions of BrO*
154 *and IO with NO result in a change in the NO₂:NO ratio of approximately 10 %, on average, which reduces the*
155 *impact of HO₂ + NO as both a sink for HO₂ and a source for OH.*

156

157 **Minor Comments: P2,L54: “ in in HO_x.”, please remove one “in”.**

158

159 We have corrected this.

160

161 **P3,L81: please replace “troposphere” by tropospheric?**

162

163 We have changed this sentence to:

164

165 *In general, observationally constrained box model simulations suggest that halogens in the troposphere will*
166 *increase OH concentrations.*

167

168 **P31, Fig.1: For clarity, please improve quality in the box model results, e.g. what represents the yellow color?**

169

170 The yellow data points represent the box model concentrations including halogen chemistry. We have corrected
171 the figure caption, which previously stated the points to be orange, and have made some improvements to the
172 presentation of the figure (symbol size, scale) to improve the clarity. Additional plots also are provided in the
173 supplementary material to show these data in more detail

174

175 **Impacts of bromine and iodine chemistry on tropospheric OH and HO₂:**
176 **Comparing observations with box and global model perspectives**

177
178 **Daniel Stone,¹ Tomás Sherwen,² Mathew J. Evans,^{2,3} Stewart Vaughan,¹ Trevor Ingham,^{1,4}**
179 **Lisa K. Whalley,^{1,4} Peter M. Edwards,² Katie A. Read,^{2,3} James D. Lee,^{2,3} Sarah J. Moller,^{2,3}**
180 **Lucy J. Carpenter,^{2,3} Alastair C. Lewis,^{2,3} Dwayne E. Heard^{1,4}**

181
182 ¹ School of Chemistry, University of Leeds, Leeds, UK

183 ² Wolfson Atmospheric Chemistry Laboratories, Department of Chemistry, University of York, York, UK

184 ³ National Centre for Atmospheric Science, University of York, York, UK

185 ⁴ National Centre for Atmospheric Science, University of Leeds, Leeds, UK

186
187
188 **Abstract**

189 The chemistry of the halogen species bromine and iodine has a range of impacts on tropospheric composition,
190 and can affect oxidising capacity in a number of ways. However, recent studies disagree on the overall sign of
191 the impacts of halogens on the oxidising capacity of the troposphere. We present simulations of OH and HO₂
192 radicals for comparison with observations made in the remote tropical ocean boundary layer during the Seasonal
193 Oxidant Study at the Cape Verde Atmospheric Observatory in 2009. We use both a constrained box model, using
194 detailed chemistry derived from the Master Chemical Mechanism (v3.2), and the three-dimensional global
195 chemistry transport model GEOS-Chem. Both model approaches reproduce the diurnal trends in OH and HO₂.
196 Absolute observed concentrations are well reproduced by the box model but are overpredicted by the global
197 model, potentially owing to incomplete consideration of oceanic sourced radical sinks. The two models, however,
198 differ in the impacts of halogen chemistry. In the box model, halogen chemistry acts to increase OH
199 concentrations (by 9.8 % at midday at Cape Verde), while the global model exhibits a small increase in OH at
200 Cape Verde (by 0.6 % at midday) but overall shows a decrease in the global annual mass weighted mean OH of
201 4.5 %. These differences reflect the variety of timescales through which the halogens impact the chemical system.
202 On short timescales, photolysis of HOBr and HOI, produced by reactions of HO₂ with BrO and IO, respectively,
203 increases the OH concentration. On longer timescales, halogen catalysed ozone destruction cycles lead to lower
204 primary production of OH radicals through ozone photolysis, and thus to lower OH concentrations. The global
205 model includes more of the longer timescale responses than the constrained box model and overall the global
206 impact of the longer timescale response (reduced primary production due to lower O₃ concentrations) overwhelms
207 the shorter timescale response (enhanced cycling from HO₂ to OH), and thus the global OH concentration
208 decreases. The Earth system contains many such responses on a large range of timescales. This work highlights
209 the care that needs to be taken to understand the full impact of any one process on the system as a whole.

210 Introduction

211 Halogen chemistry in the troposphere influences budgets of O₃, HO_x (OH and HO₂), NO_x (NO and NO₂) (von
212 Glasow et al., 2004; Saiz-Lopez and von Glasow, 2012; Simpson et al., 2015, Schmidt et al., 2016; Sherwen et
213 al., 2016a; Sherwen et al., 2016b), affects the oxidation state of atmospheric mercury (Holmes et al., 2006; Holmes
214 et al., 2010), and impacts aerosol formation (Hoffmann et al., 2001; O'Dowd et al., 2002; McFiggans et al., 2004;
215 McFiggans et al., 2010; Mahajan et al., 2011; Sherwen et al., 2016c).

216
217 The production of bromine and iodine atoms in the marine boundary layer (MBL) following emissions of
218 organohalogen compounds and the inorganic compounds I₂ and HOI has been shown to result in considerable
219 destruction of tropospheric ozone (Read et al., 2008), leading to the production of bromine monoxide (BrO) and
220 iodine monoxide (IO) radicals. Observations of BrO and IO radicals within the MBL have demonstrated
221 widespread impacts on atmospheric composition and chemistry (Alicke et al., 1999; Sander et al., 2003; Leser et
222 al., 2003; Saiz-Lopez and Plane, 2004; Saiz-Lopez et al., 2004; Peters et al., 2005; Saiz-Lopez et al., 2006;
223 Whalley et al., 2007; Mahajan et al., 2010a; Commane et al., 2011; Dix et al., 2013; Gomez Martin et al., 2013;
224 [Le Breton et al., 2017](#)), including significant effects on HO_x concentrations and on the HO₂:OH ratio in coastal
225 and marine locations (Bloss et al., 2005a; Sommariva et al., 2006; Bloss et al., 2007; Bloss et al., 2010; Kanaya
226 et al., 2007; Whalley et al., 2010).

227
228 The role of halogens in HO_x chemistry was demonstrated during the NAMBLEX campaign in Mace Head,
229 Ireland, (Heard et al., 2006), following several studies which attributed box model overestimates of HO₂
230 observations in marine environments to unmeasured halogen monoxides (Carslaw et al., 1999; Carslaw et al.,
231 2002; Kanaya et al., 2001; Kanaya et al., 2002; Kanaya et al., 2007). Simultaneous measurements of OH and HO₂
232 by laser-induced fluorescence (LIF) (Bloss et al., 2005a; Smith et al., 2006) and halogen species by a combination
233 of DOAS (for BrO or IO, OIO and I₂) (Saiz-Lopez et al., 2006) and broadband cavity ringdown spectroscopy
234 (BBCRDS) (for OIO and I₂) (Bitter et al., 2005) during NAMBLEX enabled box model calculations to fully
235 explore the impacts of halogens on the local composition. A box model without halogen chemistry was able to
236 reproduce the NAMBLEX OH observations to within 25 %, but HO₂ observations were overestimated by up to a
237 factor of 2 (Sommariva et al., 2006). The introduction of halogen chemistry, using DOAS measurements of BrO
238 and IO (Saiz-Lopez et al., 2006) to constrain the model, increased the modelled OH concentrations by up to 15
239 % and decreased HO₂ by up to 30 % owing to reactions of HO₂ with XO radicals to form HOX which subsequently
240 photolysed to X + OH (Sommariva et al., 2006). Bloss et al., (2005a) indicated that up to 40 % of the instantaneous
241 HO₂ loss could be attributed to HO₂ + IO, and that photolysis of HOI was responsible for 15 % of the noontime
242 OH production.

Deleted: in

244 The impacts of halogen chemistry on HO_x radicals at a site representative of the open ocean have been investigated
245 at the Cape Verde Atmospheric Observatory (CVAO). Measurements of halogen monoxides (Mahajan et al.,
246 2010a) at the site have been shown to have significant impacts on local ozone concentrations, notably in the
247 magnitude of the daily cycle (Read et al., 2008), and have been used to constrain box model calculations used to
248 explore observations of OH and HO₂ made during the RHaMBLe campaign in 2007 (Whalley et al., 2010). The
249 model calculations showed generally good comparisons with the observed OH and HO₂ concentrations, apart
250 from a period characterised by unusually high concentrations of HCHO. Compared to a model run in which
251 halogen chemistry was absent, bromine and iodine chemistry led to a 9 % increase in the modelled OH
252 concentration (Whalley et al., 2010). Owing to the dominance of the tropics in global methane oxidation (Bloss
253 et al., 2005b), such an impact of halogens on OH could have significant consequences for estimates of global
254 methane lifetimes, and on our understanding of the impacts of halogen chemistry on climate change.

255
256 In general, observationally constrained box model simulations suggest that halogens in the troposphere will
257 increase OH concentrations, primarily because of a change in the HO₂ to OH ratio occurring as a result of reactions
258 of halogen oxides (XO) with HO₂ to produce a hypohalous acid (HOX) which photolyses to give an OH radical
259 and a halogen atom (Kanaya et al., 2002; Bloss et al., 2005a; Kanaya et al., 2007; Sommariva et al., 2006;
260 Sommariva et al., 2007; Whalley et al., 2010). Other impacts on the HO_x photochemical system are observed
261 (impacts from changes to NO_x chemistry etc.) but these are minor and overall the general conclusion is that the
262 halogen chemistry tends to increase the OH concentration and thus the oxidising capacity of the atmosphere.

263
264 However, the observationally constrained studies are typically concerned with processes occurring at the surface,
265 and in a single location. The role of halogen chemistry in the troposphere as a whole is more uncertain, particularly
266 in the free troposphere and on a global scale (Saiz-Lopez and von Glasow, 2012; Simpson et al., 2015). Inclusion
267 of bromine chemistry in the three-dimensional (3D) chemistry transport model (CTM) MATCH-HPIC resulted
268 in decreases in tropospheric ozone concentrations of ~18 % over widespread areas, with regional decreases of up
269 to 40 % (von Glasow et al., 2004). Increases of more than 20 % were found for OH in the free troposphere, but,
270 globally, changes to OH were dominated by decreases in OH in the tropics owing to a reduction in primary
271 production from O₃ photolysis, leading to a decrease of 1-2 % in the global mean OH concentration (von Glasow
272 et al., 2004).

273
274 Significant decreases in tropospheric ozone (up to 30% at high latitude spring) were also reported for the
275 pTOMCAT model on inclusion of bromine chemistry (Yang et al., 2005). The CAM-Chem global chemistry-
276 climate model has shown an approximate 10 % decrease in global mean tropospheric ozone concentration on

Deleted: chemistry

278 incorporation of lower bromine emissions (Saiz-Lopez et al., 2012), while the GEOS-Chem CTM displays a
279 global decrease of 6.5 % (Parrella et al., 2012). The GEOS-Chem model indicated that bromine-catalysed loss
280 of ozone is limited by the rate of production of HOBr, and that HO₂ + BrO is responsible for over 95 % of the
281 global tropospheric HOBr production. While HOBr can act as a source of OH on photolysis, the changes to O₃
282 and NO_x resulting from the inclusion of bromine chemistry in GEOS-Chem led to a 4 % decrease overall in the
283 global annual mean OH (Parrella et al., 2012).

284
285 Vertically resolved airborne measurements of IO radicals in the free troposphere over the Pacific Ocean have also
286 demonstrated a role for iodine chemistry throughout the free troposphere, with IO observed at a mixing ratio of
287 ~0.1 ppt in the free troposphere and found to be present in both recent deep convective outflow and aged free
288 tropospheric air (Dix et al., 2013). Model simulations to investigate iodine-driven ozone destruction throughout
289 the troposphere indicated that only 34 % of the total iodine-driven ozone loss occurs within the marine boundary
290 layer, with 40 % occurring in a transition layer and 26 % in the free troposphere (Dix et al., 2013).

291
292 The CAM-Chem and GEOS-Chem models have also been updated to encompass iodine chemistry, with results
293 from CAM-Chem showing iodine chemistry to be responsible for 17-27 % of the ozone loss in the tropical MBL
294 and 11-27 % of the ozone loss in the marine upper troposphere (Saiz-Lopez et al., 2014). The GEOS-Chem model
295 also showed iodine chemistry to be responsible for significant ozone destruction throughout the troposphere
296 (Sherwen et al., 2016a; Sherwen et al., 2016b; Sherwen et al., 2017). The GEOS-Chem simulations, which
297 incorporate chlorine, bromine and iodine chemistry, show a reduction in global tropospheric ozone concentration
298 of 18.6 %, compared to simulations with no halogen chemistry, a reduction in the global mean OH of 8.2 % to a
299 concentration of $1.28 \times 10^6 \text{ cm}^{-3}$ and a resulting increase in global methane lifetime of 10.8 % to 8.28 years
300 (Sherwen et al., 2016b).

301
302 There is thus a discrepancy between box and global models as to the impact of halogen chemistry on OH
303 concentrations in the troposphere. Box models suggesting that OH radical concentrations should increase and
304 thus that halogens tend to increase the oxidising capacity, whereas the global models tend to suggest the opposite.

305
306 In this work, we use both a detailed chemical box model approach and a global chemistry-transport model to
307 investigate the local and global impacts of halogen chemistry on HO_x radical concentrations. We focus on
308 seasonal HO_x observations available from the Cape Verde Atmospheric Observatory (Vaughan et al., 2012). We
309 first provide a summary of the measurement site and the observations, followed by details of the two models used

310 in this study. We then evaluate the impact of halogens on the concentrations of oxidants in the two modelling
311 frameworks and consider the impact of halogen chemistry on global oxidising capacity.

313 **The Cape Verde Atmospheric Observatory**

314 The Cape Verde Atmospheric Observatory is situated on the north east coast of the island of Sao Vicente (16.848
315 °N, 24.871 °W), approximately 500 km off the west coast of Africa. The observatory is in a region of high marine
316 biological production, and, for 95 % of the time, receives the prevailing northeasterly trade wind directly off the
317 ocean (Read et al., 2008; Carpenter et al., 2010). Measurements at the observatory are considered to be
318 representative of the open ocean, and CO, O₃, VOCs, NO_x and NO_y have been measured near-continuously at the
319 observatory since October 2006 (Lee et al., 2009; Carpenter et al., 2010).

320
321 In 2007, the observatory was host to the RHaMBLe intensive field campaign, during which a number of additional
322 measurements were made to complement the long-term measurements at the site (Lee et al., 2010), including LP-
323 DOAS measurements of halogen species (Read et al., 2008; Mahajan et al., 2010a) and formaldehyde (Mahajan
324 et al., 2010b), and LIF-FAGE measurements of OH and HO₂ (Whalley et al., 2010). The halogen monooxide
325 radicals BrO and IO exhibited a ‘top-hat’ diurnal cycle (Vogt et al., 1999; Vogt et al., 1996; Read et al., 2008;
326 Mahajan et al., 2010a) with essentially zero concentration in the hours of darkness and generally constant values
327 of approximately 2.5 ppt BrO and 1.4 ppt IO during the day.

328
329 The RHaMBLe campaign was followed by the Seasonal Oxidants Study (SOS) in 2009, during which
330 measurements of OH and HO₂ were conducted over three periods (Feb-March (SOS1), May-June (SOS2), and
331 September (SOS3)), and are discussed in detail by Vaughan et al. (2012). We present here the results from a
332 modelling study of the HO_x measurements made during SOS1 and SOS2, when supporting measurements are
333 available, using both box and global model approaches. SOS3 is not considered in this work owing to a lack of
334 supporting measurements.

335
336 Measurements of OH and HO₂ during the Seasonal Oxidant Study were made by laser-induced fluorescence (LIF)
337 spectroscopy at low pressure using the fluorescence assay by gas expansion (FAGE) technique, and are described
338 in detail by Vaughan et al. (2012). Briefly, ambient air is drawn into a fluorescence cell situated on the roof of a
339 shipping container and maintained at pressures of ~ 2 Torr. The fluorescence cell has two excitation axes, with
340 excess NO added at the second axis to titrate HO₂ to OH, enabling simultaneous detection of OH and HO₂. OH
341 radicals in both excitation axes are excited by laser light at $\lambda \sim 308$ nm, generated by frequency tripling the output

342 of a solid state Nd:YAG pumped Ti:Sapphire laser system (Bloss et al., 2003). Channel photomultiplier tubes
343 coupled to gated photon counters are used to detect the $A^2\Sigma^+ - X^2\Pi_i$ OH fluorescence signal at $\lambda \sim 308$ nm.

344
345 Calibration of the instrument is achieved by measurement of the fluorescence signal from known concentrations
346 of OH and HO₂, produced by the photolysis of water vapour, and was performed over a range of conditions before,
347 during and after the campaign. For OH, the 1 σ limit of detection (LOD) was in the range $(2-11) \times 10^5$ cm⁻³ for a
348 5 min averaging period, while for HO₂ 1 σ LOD was in the range $(6-13) \times 10^5$ cm⁻³ for a 4 min averaging period.
349 Uncertainties (2 σ) in the measurements of OH and HO₂ are ~ 32 % (Vaughan et al., 2012).

350
351 Potential interferences in HO₂ measurements arising from conversion of alkene- and aromatic-derived peroxy
352 radicals to OH within the LIF detection cell, as described by Fuchs et al. (2011), are expected to be small for this
353 work owing to relatively low concentrations of alkenes and aromatics at the Cape Verde observatory (Carpenter
354 et al., 2010; Vaughan et al., 2012). Speciation of the peroxy radicals in the box model output (see Supplementary
355 Material) shows that 87.4 % of the peroxy radicals are HO₂ and CH₃O₂, 6.5 % CH₃C(O)O₂ and 1.1 % C₂H₅O₂,
356 all of which display no HO₂ interference in the laboratory (Whalley et al., 2013; Stone et al., 2014). Peroxy
357 radicals derived from OH-initiated oxidation of ethene and propene (HOC₂H₄O₂ and HOC₃H₆O₂, respectively)
358 were found to result in an interference signal for HO₂ in the laboratory (~ 40 % for the experimental configuration
359 in this work) but each radical comprises only ~ 0.6 % of the total RO₂ in this work. Thus, model calculations
360 reported here do not include representation of potential HO₂ interferences, although such phenomena may be
361 important in other environments (see for example, Whalley et al., 2013; Stone et al., 2014).

362 363 **Model Approaches**

364 We interpret the observations using two different modeling frameworks. The first is an observationally
365 constrained box model (DSMACC), the second is a global tropospheric chemistry transport model (GEOS-
366 Chem).

367 368 **Constrained Box Model**

369 The Dynamically Simple Model of Atmospheric Chemical Complexity (DSMACC) is described in detail by
370 Emmerson and Evans (2009) and Stone et al. (2010), and is a zero-dimensional model using the Kinetic Pre-
371 Processor (KPP) (Sandu and Sander, 2006). In this work we use a chemistry scheme based on a subsection of the
372 hydrocarbons (ethane, propane, *iso*-butane, *n*-butane, *iso*-pentane, *n*-pentane, hexane, ethene, propene, 1-butene,
373 acetylene, isoprene, toluene, benzene, methanol, acetone, acetaldehyde and DMS) available from the Master
374 Chemical Mechanism version 3.2 (MCM v3.2 <http://mcm.leeds.ac.uk/MCM/home.htm>) (Jenkin et al., 2003;

375 Saunders et al., 2003), with a halogen chemistry scheme described by Saiz-Lopez et al. (2006), Whalley et al.
376 (2010) and Edwards et al. (2011). We also include the reaction between OH and CH₃O₂ (Bossolasco et al., 2014;
377 Fittschen et al., 2014; Assaf et al., 2016; Yan et al., 2016), with a rate coefficient of $1.6 \times 10^{-10} \text{ cm}^3 \text{ s}^{-1}$ (Assaf et
378 al., 2016) and products HO₂ + CH₃O (Assaf et al., 2017), the impact of which on the HO₂:OH ratio and CH₃O₂
379 budget is described in the Supplementary Material. The total number of species in the model is ~1200, with ~5000
380 reactions. The full chemistry scheme used in the model is given in the Supplementary Data.

381

382 All measurements are merged onto a 10 minute timebase for input to the model and the model is run with
383 constraints applied as discussed in our previous work (Stone et al., 2010; Stone et al., 2011; Stone et al., 2014).
384 Concentrations of CH₄ and H₂ are kept constant at values of 1770 ppb (NOAA CMDL flask analysis,
385 <ftp://ftp.cmdl.noaa.gov/ccg/ch4/>) and 550 ppb (Ehhalt and Rohrer, 2009; Novelli et al., 1999) respectively.
386 Formaldehyde measurements were not available during the SOS and we thus use HCHO concentrations generated
387 by the chemistry in the model, with the modelled HCHO concentrations in broad agreement with previous
388 measurements at the observatory (Mahajan et al., 2010b). Table 1 shows a summary of the input parameters to
389 the model.

Species	Mean	Median	Range
O₃ / ppb	33.8 ± 8.6	30.7	19.6 – 49.7
CO / ppb	102.3 ± 10.3	99.3	87.8 – 127.3
H₂O / ppm	20542.3 ± 2753.8	21290.0	16778.5 – 24909.2
NO / ppt	11.2 ± 10.6	9.0	0.06 – 96.2
Ethane / ppt	961.3 ± 289.4	864.0	625.4 – 1799.2
Propane / ppt	136.1 ± 87.05	111.8	20.2 – 521.5
iso-butane / ppt	13.4 ± 9.8	11.1	0 – 62.7
n-butane / ppt	21.9 ± 17.6	17.8	0 – 112.9
Acetylene / ppt	79.0 ± 27.8	70.4	45.0 – 180.5
Isoprene / ppt	0.1 ± 0.4	0	0 – 2.6
iso-pentane / ppt	3.9 ± 3.2	3.3	0 – 22.9
n-pentane / ppt	4.3 ± 3.0	3.9	0 – 21.7
n-hexane / ppt	1.0 ± 0.7	0.9	0 – 4.4
Ethene / ppt	43.6 ± 15.2	46.3	6.4 – 73.2
Propene / ppt	13.5 ± 3.6	13.0	6.2 – 24.1
But-1-ene / ppt	6.5 ± 1.4	6.3	3.5 – 10.6
Benzene / ppt	13.0 ± 17.0	8.3	0 – 64.4
Toluene / ppt	77.9 ± 388.8	0	0 – 2013.9
Acetaldehyde / ppt	511.8 ± 526.0	599.3	0 – 2622.6
Methanol / ppt	247.6 ± 336.2	173.3	0 – 3337.4
DMS / ppt	8.3 ± 38.3	0	0 – 291.8

Table 1: Summary of inputs to the model. Zero values indicate measurements below the limit of detection. Further details can be found in Vaughan et al. (2012) and Carpenter et al. (2010).

400 Deposition processes, including dry deposition and wet deposition, and diffusion are represented in the model by
401 a first-order loss process, with the first-order rate coefficient equivalent to a lifetime of approximately 24 hours,
402 As discussed by Stone et al. (2010), variation of the deposition lifetime between 1 hour and 5 days results in
403 limited changes to the modelled concentrations of OH and HO₂. Loss of reactive species to aerosol surfaces is
404 represented in the model by parameterisation of a first-order loss process to the aerosol surface (Schwarz, 1986),
405 as discussed by Stone et al. (2014).

Deleted: Physical loss of each species in the model is

Deleted: .

Deleted: as

406
407 A range of aerosol uptake coefficients for HO₂ have been reported in the literature, with recent measurements
408 indicating values of γ_{HO_2} between 0.003 and 0.02 on aqueous aerosols (George et al., 2013) while others have
409 reported values of $\gamma_{\text{HO}_2} \sim 0.1$ (Taketani et al., 2008), and increased uptake coefficients in the presence of Cu and
410 Fe ions (Thornton et al., 2008; Mao et al., 2013). In this work we use a value of $\gamma_{\text{HO}_2} = 0.1$ in order to maintain
411 consistency with previous modelling studies at the site (Whalley et al., 2010) and to account for potential impacts
412 of ions of copper and iron in aerosol particles influenced by mineral dust (Carpenter et al., 2010; Muller et al.,
413 2010; Fomba et al., 2014; Matthews et al., 2014; Lakey et al., 2015).

414
415 The aerosol surface area in the model is constrained to previous measurements of dry aerosol surface area at the
416 observatory, corrected for differences in sampling height between the aerosol and HO_x measurements and for
417 aerosol growth under humid conditions (Allan et al., 2009; Muller et al., 2010; Whalley et al., 2010).

418
419 Halogen species are constrained to a 'top-hat' profiles for BrO and IO (Vogt et al., 1999; Vogt et al., 1996; Read
420 et al., 2008), as observed during the RHAMBLE campaign in 2007 (Read et al., 2008; Mahajan et al., 2010a).
421 The observations indicate that while there is day to day variation in BrO and IO concentrations, there is little
422 seasonal variation (Mahajan et al., 2010a). BrO and IO are thus constrained to the mean observed mixing ratios
423 of 2.5 ppt and 1.4 ppt, respectively, for time points between 0930 and 1830 (GMT) and zero for all other times.
424 Sensitivity to these mixing ratios is discussed in the Supplementary Material. In a similar way to NO_x (see Stone
425 et al. (2010; 2011)), concentrations of all bromine or iodine species, including BrO and IO, are permitted to vary
426 according to the photochemistry as the model runs forwards. At the end of each 24 hour period in the model, the
427 calculated concentrations of BrO and IO are compared to the constrained value, and the concentrations of all
428 bromine (Br, Br₂, BrO, HBr, HOBr, BrONO₂, BrNO₂, BrNO) and iodine (I, I₂, IO, HI, HOI, INO, INO₂, IONO₂,
429 OIO, I₂O₂, I₂O₃, I₂O₄, HOIO₂) species are fractionally increased or decreased such that the calculated and
430 constrained concentrations of BrO and IO are the same. The model is run forwards in time with diurnally varying
431 photolysis rates until a diurnal steady state is reached, typically requiring between 5 and 10 days.

Global Model

We use the 3D global chemistry transport model GEOS-Chem (v10-01, www.geos-chem.org). The model has been extensively evaluated against observations (Bey et al., 2001; Evans and Jacob, 2005; Nassar et al., 2009; Mao et al., 2010; Zhang et al., 2010; Parrella et al., 2012; Hu et al., 2017). The model is driven by assimilated winds calculated by the Goddard Earth Observing System at a horizontal resolution of $4^\circ \times 5^\circ$, with 47 vertical levels from the surface to 50 hPa. Anthropogenic emissions of CO, NO_x and SO₂ are described by the EDGAR 3.2 monthly global inventory (Olivier et al., 2005). Emissions of volatile organic compounds (VOCs) are described by the RETRO monthly global inventory (van het Bolscher, 2008) for anthropogenic sources, with ethane emissions described by Xiao et al., 2008, and the MEGAN v2.1 inventory (Guenther et al., 2006; Barkley et al., 2011) for biogenic sources.

The HO_x-NO_x-VOC-O₃ chemistry scheme in the model is described in detail by Bey et al. (2001) and Mao et al. (2013), with the isoprene oxidation mechanism described by Paulot et al. (2009). Photolysis rates use the FAST-JX scheme (Bian and Prather, 2002; Mao et al., 2010), with acetone photolysis rates updated by Fischer et al. (2012). Stratospheric chemistry is based on LINOZ McLinden et al. (2000) for O₃ and a linearised mechanism for other species as described by Murray et al. (2012).

The model framework includes gas-aerosol partitioning of semi-volatile organic compounds (Liao et al., 2007; Henze et al., 2007; Henze et al., 2009; Fu et al., 2008; Heald et al., 2011; Wang et al., 2011), and heterogeneous chemistry (Jacob, 2000). Coupling between gas phase chemistry and sulfate-ammonium-nitrate aerosol is described by Park et al. (2004) and Pye et al. (2009). A description of dust aerosol in the model is given by Fairlie et al. (2007). Treatment of sea salt aerosol is described by Jaegle et al. (2011). The uptake coefficient for N₂O₅ uses the parameterisation by Evans and Jacob (2005), while that for HO₂ uses the parameterisation of Thornton et al. (2008). A full description of the organic aerosol chemistry in the model is given by Heald et al. (2011).

The model includes recent updates to the chemistry scheme to include bromine chemistry (Parella et al., 2012; Schmidt et al., 2016) and iodine chemistry (Sherwen et al., 2016a; Sherwen et al., 2016b). Sources of tropospheric bromine in the model include emissions of CHBr₃, CH₂Br₂ and CH₃Br, and transport of reactive bromine from the stratosphere. Debromination of sea-salt aerosol is not included in the model following the work of Schmidt et al. (2016), which showed better agreement with observations of BrO made by the GOME-2 satellite (Theys et al., 2011) and in the free troposphere and the tropical Eastern Pacific MBL (Gomez Martin et al., 2013; Volkamer et al., 2015; Wang et al., 2015). Emission rates and bromine chemistry included in the model are described in detail by Parella et al. (2012), with the bromine chemistry scheme described by 19 bimolecular reactions, 2 three-body

Deleted: ¶
¶

Deleted: additional

472 reactions and 2 heterogeneous reactions using rate coefficients, heterogeneous reaction coefficients and photolysis
473 cross-sections recommended by Sander et al. (2011).

474

475 Iodine sources include emissions of CH₃I, CH₂I₂, CH₂ICl, CH₂IBr, I₂ and HOI. Emissions for CH₃I follow Bell
476 et al. (2002), while those of other organic iodine species use parameterisations based on chlorophyll-a in the
477 Tropics and constant oceanic and coastal fluxes in extratropical regions (Ordóñez et al., 2012). Emissions of
478 inorganic iodine species (HOI and I₂) use the results of Carpenter et al. (2013), with oceanic iodide concentrations
479 parameterised by MacDonald et al. (2014). The iodine chemistry scheme includes 26 unimolecular and
480 bimolecular reactions, 3 three-body reactions, 21 photolysis reactions and 7 heterogeneous reactions, using
481 recommendations by Atkinson et al. (2007) and Sander et al. (2011) where available. Full details are given by
482 Sherwen et al. (2016a; 2016b).

483

484 Photolysis rates of bromine and iodine compounds are calculated using the FAST-J radiative transfer model (Wild
485 et al., 2000; Bian and Prather, 2002; Mao et al., 2010). Wet and dry deposition are determined as for the standard
486 GEOS-Chem model (Liu et al., 2001; Wesely, 1989; Wang et al., 1998; Amos et al., 2012).

487

488 The tropospheric chemistry scheme is integrated using the SMVGEAR solver (Jacobson and Turco, 1994; Bey et
489 al., 2001). The model, provides hourly output at the site of the Cape Verde Atmospheric Observatory. Model
490 simulations have been performed in the absence of halogens, with bromine chemistry, with iodine chemistry and
491 with bromine and iodine chemistry combined. Each model simulation is run for two years, with the analysis
492 performed on the second year (2009) and the first year discarded as model spin-up to enable evolution of long-
493 lived species.

494

495 **Model Results**

496 We now investigate the impact of halogen chemistry on tropospheric oxidation at Cape Verde within our two
497 modelling approaches.

498

499 **Constrained Box Model**

500 Figure 1 shows the observed and modelled time series for OH and HO₂ during SOS1 (February, March 2009) and
501 SOS2 (May, June 2009). Observed concentrations of OH and HO₂ were typically higher in SOS2 than SOS1,
502 reaching maximum values in SOS2 of $\sim 9 \times 10^6 \text{ cm}^{-3}$ OH and $4 \times 10^8 \text{ cm}^{-3}$ HO₂ (Vaughan et al., 2012). Similar
503 concentrations were observed in May and June 2007 during the RHaMBLe campaign (Whalley et al., 2010), with
504 a *t*-test indicating no statistically significant difference between the OH concentrations measured in May-June

505 2009 to those measured in May-June 2007 at the 95 % confidence level (Vaughan et al., 2012). Concentrations
506 of HO₂ measured in May-June 2009 were significantly higher than those measured in May-June 2007 at the 95
507 % confidence level, but were within the 1σ day-to-day variability (Vaughan et al., 2012). Temperatures during
508 SOS2 were typically higher than those during SOS1, with higher relative humidity during SOS2 (Vaughan et al.,
509 2012). Air masses during SOS1 had strong contributions from Atlantic marine air and African coastal region,
510 with polluted marine air and Saharan dust contributing ~ 20 % and 10 %, respectively, for the first half of the
511 measurement period. Conditions during SOS2 were typically cleaner, with Atlantic marine air representing the
512 major source, although coastal African air contributed ~ 40 % on some days. There was little influence from
513 polluted air, dust or continental air (Vaughan et al., 2012). Analysis of the variance of OH and HO₂ during SOS
514 indicated that ~70 % of the total variance could be explained by diurnal behaviour, with the remaining ~30 %
515 related to changes in air mass.

516

517 Figure 1 shows the observed and modelled time series for OH and HO₂, for model simulations with and without
518 halogen chemistry. For SOS1, the box model overpredicts the OH and HO₂ concentrations at the start of the
519 campaign (Julian days 59 and 61), but performs better for day 63, and captures both the observed diurnal profile
520 and the observed concentrations. For SOS2, the box model tends to agree better with the observations for both
521 OH and HO₂. A day-by-day comparison between the models and the observations is shown in the Supplementary
522 Material for days for which box model calculations were possible, which were limited by the availability of
523 supporting data.

524

525 Figure 2 shows the point-by-point model performance for OH and HO₂ for all data points combined, and for
526 SOS1 and SOS2 separately, for the full box model run including halogen chemistry. There is a tendency for
527 overprediction of OH and HO₂ during SOS1 (slopes of modelled vs observed concentrations are (1.86 ± 0.26) for
528 OH and (1.66 ± 0.21) for HO₂), which is dominated by the model overpredictions on days 59 and 61, with better
529 agreement observed during SOS2 (slopes of modelled vs observed concentrations are (1.11 ± 0.15) for OH and
530 (1.21 ± 0.12) for HO₂).

531

532 The measured and modelled average diurnal profiles of OH, HO₂ and the HO₂ to OH ratios are shown in Figure
533 3. At midday (1100-1300), the full model including halogen chemistry overpredicts OH by a median factor of
534 1.52 and HO₂ by a median factor of 1.21. A model run containing bromine chemistry but no iodine chemistry
535 gave median midday overpredictions of 1.40 and 1.30 for OH and HO₂, respectively, while a run containing
536 iodine but not bromine gave equivalent median overpredictions of 1.50 and 1.26, respectively. With no halogen
537 chemistry included in the model, the modelled OH decreases, giving a median overprediction at midday by a

538 factor of 1.37, while the modelled HO₂ increases, resulting in a median overprediction by a factor of 1.37 at
539 midday.

540

541 Thus the inclusion of halogens (bromine and iodine) in the box model changes the mean noon time OH and HO₂
542 concentrations by +9.8 % and -9.9 %, respectively. This impact of halogen chemistry is consistent in sign and
543 magnitude with previous studies (Kanaya et al., 2002; Bloss et al., 2005a; Kanaya et al., 2007; Sommariva et al.,
544 2006; Sommariva et al., 2007; Whalley et al., 2010).

545

546 Figure 4 shows the mean midday total RO_x budget (given the fast processing time between HO₂ and HOBr/HOI
547 we identify the RO_x family as OH, HO₂, HOBr, HOI, RO and RO₂) for the two measurement periods during SOS
548 for model runs with and without halogens. These budgets are similar both between time periods (i.e. SOS1 vs
549 SOS2) and for box model calculations with and without halogen chemistry. Radical production dominated by
550 photolysis of ozone (~83 %), with photolysis of HCHO (~10 %), CH₃CHO (~2 %) and H₂O₂ (~2 %) playing a
551 significantly smaller role. Radical termination reactions were dominated by HO₂ + CH₃O₂ (~23 %), aerosol uptake
552 of HO₂ (~21 %), HO₂ + HO₂ (~19 %), CH₃C(O)O₂ + HO₂ (~8 %), and OH + HO₂ (~5 %). The inclusion of the
553 reaction between OH and CH₃O₂ reduces the importance of radical termination via HO₂ + CH₃O₂ (from ~26 %
554 of the total to ~23 % of the total), but otherwise has little impact on the total radical removal owing to the expected
555 production of HO₂ + CH₃O (Assaf et al., 2017). Further details regarding the impact of the reaction between OH
556 and CH₃O₂ on the HO₂:OH ratio and CH₃O₂ budget are given in the Supplementary Material.

557

558 The budget analyses for SOS are consistent with those determined for the RHAMBLE campaign (Whalley et al.,
559 2010; Fittschen et al., 2014; Assaf et al., 2017), reflecting similarities in observed concentrations of long-lived
560 species and the method of the model constraint with observed O₃ concentrations and photolysis rates. The primary
561 source of radicals therefore remains fixed in all simulations, with the primary sinks for these species occurring
562 through radical-radical reactions. Thus, the total radical concentration and budget is little impacted by the
563 presence of halogens.

564

565 However, the partitioning of the radicals is impacted by the halogens. Without halogens the average midday
566 (1100-1300) HO₂ to OH ratio is (83.4 ± 15.4) (median = 82.7), with the halogens this changes to (68.3 ± 13.6)
567 (median = 66.9) (Table 2). This change in partitioning is mainly due to the reaction of HO₂ with BrO and IO
568 followed by the photolysis of HOBr and HOI to give OH. In this way the halogens tend to reduce the concentration
569 of HO₂ and increase the concentration of OH.

570

HO₂:OH ratio

Observed	79.1 ± 34.1 (70.7)
Box model, no halogens	83.4 ± 15.4 (82.7)
Box model with Br chemistry	78.9 ± 15.6 (77.8)
Box model with I chemistry	71.5 ± 13.0 (70.4)
Box model with Br and I chemistry	68.3 ± 13.6 (66.9)
Global model, no halogens	80.8 ± 18.1 (78.9)
Global model with Br chemistry	81.9 ± 19.0 (79.7)
Global model with I chemistry	70.4 ± 12.5 (70.5)
Global model with Br and I chemistry	71.3 ± 13.2 (71.3)

Table 2: Mean ($\pm 1\sigma$) midday (1100-1300 hours) ratios of HO₂ to OH (SOS1 and SOS2 combined). Median values are given in parentheses.

In the box model without halogen chemistry, production of OH is dominated by ozone photolysis (76 %), HO₂ + NO (12 %) and HO₂ + O₃ (9 %), with OH loss controlled by OH + CO (37 %), OH + CH₄ (16 %) and OH + CH₃CHO (15 %), as shown in Figure 5. Production of HO₂ in the model excluding halogens is controlled by OH + CO (45 %), CH₃O + O₂ (19 %) and photolysis of HCHO (10 %), with loss governed by aerosol uptake (26 %), HO₂ + HO₂ (26 %), HO₂ + NO (15 %), HO₂ + CH₃O₂ (12 %) and HO₂ + O₃ (10 %). In the presence of halogens, the instantaneous budgets for OH and HO₂ are impacted by BrO and IO, as shown in Figures 5 and 6. For the model run including halogens, OH production is still dominated by ozone photolysis (68 %), but there are significant contributions from photolysis of HOI (10 %) and HOBr (3 %). Loss of HO₂ is also affected by the presence of the halogen species, with the dominant loss processes including aerosol uptake (20 %), HO₂ + HO₂ (19 %), HO₂ + IO (14 %), HO₂ + NO (12 %), HO₂ + CH₃O₂ (11 %), HO₂ + O₃ (8 %) and HO₂ + BrO (6 %). The change in the relative importance of HO₂ + NO on inclusion of halogens in the model results from both the increase in the total HO₂ sink, owing to the additional losses through HO₂ + BrO and HO₂ + IO, and the shift in NO_x partitioning owing to the reactions Br + NO → Br + NO₂ and IO + NO → I + NO₂. The reactions of BrO and IO with NO result in a change in the NO₂:NO ratio of approximately 10 %, on average, which reduces the impact of HO₂ + NO as both a sink for HO₂ and a source for OH. As shown in Figures 4-6 there is little difference in the radical budgets between SOS1 and SOS2.

This box modelling study is consistent with previous studies (Kanaya et al., 2002; Bloss et al., 2005a; Kanaya et al., 2007; Sommariva et al., 2007; Whalley et al., 2010; Mahajan et al., 2010a; Stone et al., 2012) in that it implies that halogen chemistry is likely to increase the OH concentration of the marine boundary layer (and potentially

595 other regions of the troposphere) as it enhances the HO₂ to OH conversion through the production of HOBr and
596 HOI. We now look at the impact of halogen chemistry on the concentrations of OH and HO₂ at Cape Verde within
597 the framework of a global atmospheric chemistry model.

598 **Global Model**

600 Figure 1 shows the time series for OH and HO₂ calculated by the global model GEOS-Chem, with the average
601 diurnal profiles shown in Figure 3. The global model displays a significant overprediction for OH and HO₂ during
602 SOS1, but exhibits reasonable skill at reproducing the observed concentrations during SOS2 and captures the
603 HO₂:OH ratio for both measurement periods. The overpredictions of OH and HO₂ in the global model likely result
604 from a combination of missing OH-sinks, particularly oxygenated volatile organic compounds (oVOCs) which
605 are currently underestimated in the global model (Millet et al., 2015), and potential overprediction of the primary
606 radical production rate owing to reductions in photolysis rates resulting from cloud cover that are not captured by
607 the global model.

609 At midday (1100-1300), the modelled to observed ratios for OH and HO₂ for the global model excluding halogen
610 chemistry are (1.52 ± 1.02) and (1.72 ± 0.80) , respectively, with a mean modelled HO₂ to OH ratio of $(80.8 \pm$
611 $18.1)$ (compared to the observed HO₂ to OH ratio of (79.1 ± 34.1)). For the global model run including bromine
612 chemistry, but not iodine, the mean midday modelled to observed ratios for OH and HO₂ are (1.48 ± 1.05) and
613 (1.69 ± 0.81) , respectively, with a mean midday modelled HO₂ to OH ratio of (81.9 ± 19.0) . Bromine chemistry
614 thus acts to decrease the concentrations of both OH and HO₂, in contrast to the box model results which show
615 increased concentrations of OH and decreased concentrations of HO₂. For the model run including iodine, but not
616 bromine, the midday modelled to observed ratios for OH and HO₂ are (1.57 ± 1.00) and (1.59 ± 0.81) , respectively,
617 with a mean midday modelled HO₂ to OH ratio of (70.4 ± 12.5) . Iodine chemistry thus results in increased OH
618 and decreased HO₂ for both the global and box model simulations at Cape Verde. Inclusion of bromine and iodine
619 chemistry combined leads to midday modelled to observed ratios of (1.53 ± 1.01) for OH and (1.57 ± 0.82) for
620 HO₂, and a mean midday modelled HO₂ to OH ratio of (71.3 ± 13.2) . These results are shown in Table 2, alongside
621 those for the box model.

623 The results from the global model at Cape Verde thus differ from those of the box model. For the box model,
624 inclusion of bromine and iodine chemistry, whether separately or combined, leads to increased OH and decreased
625 HO₂ through increased conversion of HO₂ to OH through the production and subsequent photolysis of HOBr and
626 HOI. In the global model a more complex pattern emerges. In a similar way to the box model, the HO₂
627 concentrations in the global model are decreased on inclusion of bromine and/or iodine owing to the additional

Deleted: ¶

629 loss reactions $\text{HO}_2 + \text{BrO}$ and $\text{HO}_2 + \text{IO}$. When bromine chemistry is considered in the global model in isolation
630 from iodine chemistry, the OH concentration decreases, despite the production and photolysis of HOBr. This
631 decrease occurs as a result of a reduction in the O_3 concentration in the model on inclusion of bromine chemistry
632 owing to the reaction of Br with O_3 , which leads to a decrease in the rate of primary radical production from O_3
633 photolysis and thus lower OH concentrations. The impact of the decreased radical production rate is greater than
634 that leading to increased OH production through HOBr photolysis, and the net OH concentration is reduced in
635 the global model. This effect is not observed in the box model calculations as the model runs are constrained to
636 long-lived species – including O_3 . The change in O_3 concentration on the inclusion of halogen chemistry is thus
637 not considered in the box model simulations, and the subsequent impacts of halogens consider only those changes
638 occurring on a more rapid timescale, which lead to increases in the OH concentration.

639
640 However, the inclusion of iodine chemistry in the global model does lead to increased OH concentrations at Cape
641 Verde. Direct emissions of HOI in the global model, in addition to chemical production through $\text{HO}_2 + \text{IO}$, result
642 in increased OH production through HOI photolysis as well as the repartitioning of HO_2 and OH through HOI
643 production in a similar manner to that for HOBr. However, the more rapid cycling of HO_2 to OH through the
644 more rapid production and photolysis of HOI compared to HOBr, reduces the impact of iodine chemistry on the
645 HO_2 :OH ratio compared to that for bromine chemistry. Iodine chemistry thus can reduce the OH concentration
646 similarly to bromine chemistry, through the destruction of O_3 and subsequent reduction in primary production
647 rate, but the impact is less than that for bromine, and can be offset by the direct emissions of HOI which increases
648 the production rate of OH through photolysis.

649
650 The impacts of iodine chemistry in the global model are thus more complex than those for bromine chemistry.
651 When bromine and iodine chemistry are combined in the global model there is a competition between the effects
652 of the reduction in primary production of OH, through depletion of O_3 , and the production of OH from photolysis
653 of HOBr and HOI and, for the model simulations at Cape Verde, the impacts of direct HOI emissions dominate.
654 The OH concentration is thus marginally increased compared to simulations containing no halogens, although the
655 HO_2 concentrations are significantly decreased.

656
657 The impacts of halogens on OH radical concentrations in the global model thus display a complexity that is
658 somewhat obscured in the box model simulations. Overall, the inclusion of halogens in the global model leads to
659 a slight increase in OH at Cape Verde, but, owing to the opposing effects of bromine and iodine, this result is
660 subject to the modelled concentrations of bromine and iodine species. Observations at Cape Verde made between
661 November 2006 and June 2007 indicate ‘top-hat’ profiles for BrO and IO, with average daytime mixing ratios of

2.5 ppt and 1.4 ppt, respectively, and little variability over the entire campaign (Read et al., 2008; Mahajan et al., 2010a). The global model simulations reported here predict average mixing ratios of ~0.5 ppt for BrO and ~1 ppt for IO during SOS, and thus underpredict BrO but perform well for IO. The underprediction of BrO at Cape Verde results from recent model updates which exclude emissions of bromine species from sea-salt debromination (Schmidt et al., 2016) in order to provide improved agreement with observations of BrO made by the GOME-2 satellite (Theys et al., 2011) and in the free troposphere and the tropical Eastern Pacific MBL (Gomez Martin et al., 2013; Volkamer et al., 2015; Wang et al., 2015). If sea-salt debromination were included, daytime mixing ratios of BrO at Cape Verde would be approximately 2 ppt, as shown by Parella et al. (2012) and Schmidt et al. (2016), and thus in closer agreement to the observations. Increased modelled concentrations of BrO at Cape Verde resulting from inclusion of sea-salt debromination would have a greater effect on OH and HO₂, leading to more significant decreases in OH and HO₂ when bromine chemistry is included without iodine chemistry, with the larger decrease in OH potentially off-setting the increase in OH observed when bromine and iodine chemistry are combined. However, the current model simulations do not consider the coupling between bromine and sulfur chemistry, which may represent a significant sink for reactive bromine species in the troposphere and balance sources from sea-salt debromination (Chen et al., 2017). These results thus demonstrate the need for further investigation and constraint of sources and emission rates of bromine species, and of the coupling between sulfur chemistry and reactive bromine species. We now discuss the global impacts of halogen chemistry.

Global impacts of halogen chemistry on OH and HO₂

On the global scale, concentrations of OH and HO₂ are reduced on inclusion of bromine and iodine chemistry, both individually and combined. The global mass weighted annual mean OH concentration decreases by 3.8 % on inclusion of bromine chemistry, but only 0.02 % on inclusion of iodine chemistry alone. When the chemistry of bromine and iodine is combined in the model, the global mass weighted annual mean OH concentration decreases by 4.5 %. For HO₂, the global mass weighted annual mean is decreased by 4.2 % by bromine, 5.6 % by iodine and 9.7 % by bromine and iodine combined. Figure 7 shows the probability distribution functions for the changes to OH and HO₂ concentrations for the monthly mean values for all grid boxes within the troposphere for the year. For the majority of grid boxes, concentrations of OH and HO₂ are reduced on inclusion of bromine chemistry, with iodine also generally reducing HO₂ concentrations but leading to a wider spread of changes to the OH concentration, and similar numbers of grid boxes showing increased and decreased concentrations. When bromine and iodine chemistry are combined in the model, HO₂ shows a more significant decrease than for either halogen individually, and OH, although exhibiting increased concentrations in a significant number of grid boxes, displays a greater tendency for decreased concentrations.

Deleted: The global model simulations reported here predict average mixing ratios of ~0.5 ppt for BrO and ~1 ppt for IO during SOS, and thus underpredict BrO but perform well for IO. The underprediction of BrO at Cape Verde results from recent model updates which exclude emissions of bromine species from sea-salt debromination (Schmidt et al., 2016) in order to provide improved agreement with observations of BrO made by the GOME-2 satellite (Theys et al., 2011) and in the free troposphere and the tropical Eastern Pacific MBL (Gomez Martin et al., 2013; Volkamer et al., 2015; Wang et al., 2015). We now discuss the global impacts of halogen chemistry.

706
707 Figure 8 shows the changes to the annual modelled surface layer OH and HO₂ concentrations on inclusion of
708 halogen chemistry, with annual surface layer mixing ratios of BrO and IO shown in Figure 9. The most significant
709 changes to OH and HO₂ occur over marine regions, particularly over the Southern Pacific. Smaller changes are
710 observed over land, and any increased concentrations, including those for OH over Cape Verde, can be seen to
711 occur in coastal regions where the impacts of direct HOI emissions dominate and concentrations of IO
712 concentrations are typically elevated.

713
714 Thus, overall, halogens act to reduce the oxidising capacity of the troposphere through reductions to O₃ and
715 subsequent reductions in the primary production rates of OH and HO₂, despite the slight increase in OH
716 concentration predicted by the global model at Cape Verde. Consideration of the full extent of the impacts of
717 halogens on the global oxidising capacity is hindered by uncertainties in the concentrations and distributions of
718 halogen species, and model representations of halogen processes, particularly those relating to sea salt
719 debromination, ocean iodide emissions, parameterisations of iodine recycling in aerosols and photolysis of higher
720 iodine oxides (Sherwen et al., 2016a).

722 **Conclusions**

723 Measurements of OH and HO₂ made by LIF-FAGE at the Cape Verde Atmospheric Observatory during the
724 Seasonal Oxidants Study in 2009 have been simulated by a constrained box model and a three-dimensional global
725 chemistry transport model. The observations are generally reproduced well by the box model, but are
726 overpredicted by the global model.

727
728 The oxidising capacity of the two models, as manifested by the OH concentration, shows opposing sensitivity to
729 halogens. The constrained box model shows an increase in OH concentrations with the inclusion of halogens,
730 whereas the global transport model shows a decrease in OH concentrations globally, despite a marginal decrease
731 in the OH concentration at Cape Verde. This difference between models reflects differing representation of
732 chemical timescales by the models. The box model is constrained to concentrations of long-lived compounds,
733 including O₃, and considers only impacts on short timescales, whereas the global model includes impacts
734 occurring on longer timescales. Within this context, the box model includes the short timescale impact of halogens
735 on the repartitioning of HO₂ to OH, thus increasing OH and decreasing HO₂, but does not consider the longer
736 timescale impact of halogen-mediated ozone destruction which impacts primary radical production. This
737 highlights a general problem with understanding the complex interactions within atmospheric chemistry and the
738 Earth system in general. Evaluating the impact of a small part of the system on the system as a whole can be

739 difficult and the most significant processes may occur on timescales significantly longer than those of the
740 perturbation.

741

742 **Acknowledgements**

743 This project was funded by the Natural Environment Research Council (NERC, NE/E011403/1), with support of
744 the Cape Verde Atmospheric Observatory by the National Centre for Atmospheric Science (NCAS) and the
745 SOLAS project. DS would also like to thank NERC for the award of an Independent Research Fellowship
746 (NE/L010798/1). Computational resources were provided by the NERC BACCHUS project (NE/L01291X/1)

747

748 **References**

749 Aliche, B., Hebestriet, H., Stutz, J., Platt, U.: Iodine oxide in the marine boundary layer, *Nature*, 397, 572-573,
750 1999

751

752 Allan, J.D., Topping, D.O., Good, N., Irwin, M., Flynn, M., Williams, P.I., Coe, H., Baker, A.R., Martino, M.,
753 Niedermeier, N., Wiedensohler, A., Lehmann, S., Muller, K., Herrmann, H., and McFiggans, G.: Composition
754 and properties of atmospheric particles in the eastern Atlantic and impacts on gas phase uptake
755 rates, *Atmos. Chem. Phys.*, 9, 9299–9314, 2009

756

757 Amos, H.M., Jacob, D.J., Holmes, C.D., Fisher, J.A., Wang, Q., Yantosca, R.M., Corbitt, E.S., Galarneau, E.,
758 Rutter, A.P., Gustin, M.S., Steffen, A., Schauer, J.J., Graydon, J.A., St. Louis, V.L., Talbot, R.W., Edgerton, E.S.,
759 Zhang, Y., and Sunderland, E.M: Gas-particle partitioning of Hg(II) and its effect on global mercury deposition,
760 *Atmos. Chem. Phys.*, 12, 1, 591-603, doi:10.5194/acp-12-591-2012, 2012

761

762 Assaf, E., Song, B., Tomas, A., Schoemaker, C., and Fittschen, C.: Rate constant of the reaction between CH₃O₂
763 and OH radicals revisited, *J. Phys. Chem. A*, 120, 8923-8932, 2016

764

765 Assaf, E., Sheps, L., Whalley, L., Heard, D., Tomas, A., Schoemaeker, C., and Fittschen, C.: The reaction
766 between CH₃O₂ and OH radicals: Product yields and atmospheric implications, *Environ. Sci. Technol.*, 51, 4,
767 2170-2177, doi: 10.1021/acs.est.6b06265, 2017

768

769 Atkinson, R., Baulch, D.L., Cox, R.A., Crowley, J.N., Hampson, R.F., Hynes, R.G., Jenkin, M.E., Rossi, M. J.,
770 and Troe, J.: Evaluated kinetic and photochemical data for atmospheric chemistry: Volume III – gas phase
771 reactions of inorganic halogens, *Atmos. Chem. Phys.*, 7, 981–1191, doi:10.5194/acp-7-981-2007, 2007

772

773 Barkley, M.P., Palmer, P.I., Ganzeveld, L., Arneth, A., Hagberg, D., Karl, T., Guenther, A., Paulot, F., Wennberg,
774 P.O., Mao, J.Q., Kurosu, T.P., Chance, K., Muller, J.-F., De Smedt, I., van Roozendaal, M., Chen, D., Wang,
775 Y.X., and Yantosca, R.M.: Can a “state of the art” chemistry transport model simulate Amazonian tropospheric
776 chemistry? *J. Geophys. Res. Atmos.*, 116, D16302, 1-28, doi:10.1029/2011JD015893, 2011

777

778 Bell, N., Hsu, L., Jacob, D.J., Schultz, M.G., Blake, D.R., Butler, J.H., King, D.B., Lobert, J.M., and Maier-
779 Reimer, E.: Methyl iodide: Atmospheric budget and use as a tracer of marine convection in global models, J.
780 Geophys. Res. Atmos., 107, ACH 8-1–ACH 8-12, doi:10.1029/2001jd001151, 2002
781
782 Bey, I., Jacob, D.J., Yantosca, R.M., Logan, J.A., Field, B.D., Fiore, A.M., Li, Q., Liu, H.Y., Mickley, L.J.,
783 Schultz, M.G.: Global modelling of tropospheric chemistry with assimilated meteorology: Model description and
784 evaluation, J. Geophys. Res., 106, D19, 23073-23095, 2001
785
786 Bian, H.S., and Prather, M.J.: Fast-J2: Accurate simulation of stratospheric photolysis in global chemistry models,
787 J. Atmos. Chem., 41, 3, 281-296, 2002
788
789 Bitter, M., Ball, S., Povey, I., and Jones, R.: A broadband cavity ringdown spectrometer for in-situ measurements
790 of atmospheric trace gases, Atmos. Chem. Phys., 5, 3491–3532, doi:10.5194/acp-8-3491-2005, 2005
791
792 Bloss, W.J., Lee, J.D., Johnson, G.P., Sommariva, R., Heard, D.E., Saiz-Lopez, A., Plane, J.M.C., McFiggans,
793 G., Coe, H., Flynn, M., Williams, P., Rickard, A.R., Fleming, Z.: Impact of halogen monoxide chemistry upon
794 boundary layer OH and HO₂ concentrations at a coastal site, Geophys. Res. Lett., 32, L06814,
795 doi:10.1029/2004GL022084, 2005a
796
797 Bloss, W.J., Evans, M.J., Lee, J.D., Sommariva, R., Heard, D.E., Pilling, M.J.: The oxidative capacity of the
798 troposphere: Coupling of field measurements of OH and a global chemistry transport model, Faraday. Discuss.,
799 130, 425-436, 2005b
800
801 Bloss, W.J., Lee, J.D., Heard, D.E., Salmon, Bauguitte, S.J.-B., Roscoe, H.K., Jones, A.E.: Observations of OH
802 and HO₂ radicals in coastal Antarctica, Atmos. Chem. Phys., 7, 4171-4185, 2007
803
804 Bloss, W.J., Camredon, M., Lee, J.D., Heard, D.E., Plane, J.M.C., Saiz-Lopez, A., Bauguitte, S.J.-B., Salmon,
805 R.A., Jones, A.E.: Coupling of HO_x, NO_x and halogen chemistry in the Antarctic boundary layer, Atmos. Chem.
806 Phys., 10, 10187-10290, 2010
807
808 Bossolasco, A., Farago, E.P., Schoemaker, C., and Fittschen, C.: Rate constant of the reaction between CH₃O₂
809 and OH radicals, Chem. Phys. Lett., 593, 7-13, 2014
810
811 Carpenter, L. J., Fleming, Z. L., Read, K. A., Lee, J. D., Moller, S.J., Hopkins, J., Purvis, R., Lewis, A. C., Muller,
812 K., Heinold, B., Herrmann, H., Wadinga Fomba, K., van Pinxteren, D., Muller, C., Tegen, I., Wiedensohler, A.,
813 Muller, T., Niedermeier, N., Achterberg, E. P., Patey, M. D., Kozlova, E. A., Heimann, M., Heard, D. E., Plane,
814 J. M. C., Mahajan, A., Oetjen, H., Ingham, T., Stone, D., Whalley, L., Evans, M., Pilling, M. J., Leigh, R. J.,
815 Monks, P. S., Karunaharan, A., Vaughan, S., Tschirner, J., Pöhler, D., Frieß, U., Holla, R., Mendes, L., Lopez,
816 H., Faria, B., Manning, A. J., and Wallace, D. W. R.: Seasonal characteristics of tropical marine boundary layer
817 air measured at the Cape Verde Atmospheric Observatory, J. Atmos. Chem., 67, 87–140, 2010
818

819 Carpenter, L.J., MacDonald, S.M., Shaw, M.D., Kumar, R., Saunders, R.W., Parthipan, R., Wilson, J., and Plane,
820 J.M.C.: Atmospheric iodine levels influenced by sea surface emissions of inorganic iodine, *Nat. Geosci.*, 6, 108–
821 111, doi:10.1038/ngeo1687, 2013
822
823 Carslaw, N., Creasey, D. J., Heard, D. E., Lewis, A. C., McQuaid, J. B., Pilling, M. J., Monks, P. S., Bandy, B. J.,
824 and Penkett, S. A.: Modeling OH, HO₂, and RO₂ radicals in the marine boundary layer – 1. Model construction
825 and comparison with field measurements, *J. Geophys. Res.*, 104(D23), 30 241–30 255, 1999
826
827 Carslaw, N., Creasey, D. J., Heard, D. E., Jacobs, P. J., Lee, J. D., Lewis, A. C., McQuaid, J. B., Pilling, M. J.,
828 Bauguitte, S., Penkett, S. A., Monks, P. S., Salisbury, G.: Eastern Atlantic Spring Experiment 1997 (EASE97) –
829 2. Comparisons of model concentrations of OH, HO₂, and RO₂ with measurements, *J. Geophys. Res.-Atmos.*,
830 107(D14), 4190, 2002
831
832 [Chen, Q., Schmidt, J.A., Shah, V., Jaegle, L., Sherwen, T., and Alexander, B.: Sulfate production by reactive](#)
833 [bromine: Implications for the global sulfur and reactive bromine budgets, *Geophys. Res. Lett.*, 44, 7069-7078,](#)
834 [doi:10.1002/2017GL073812, 2017](#)
835
836 Commane, R., Seitz, K., Bale, C.S.E., Bloss, W.J., Buxmann, J., Ingham, T., Platt, U., Pöhler, D., Heard, D.E.:
837 Iodine monoxide at a clean marine coastal site: observations of high frequency variations and inhomogeneous
838 distributions, *Atmos. Chem. Phys.*, 11, 6721-6733, 2011
839
840 Dix, B., Baidar, S., Bresch, J.F., Hall, S.R., Schmidt, S., Wang, S., Volkamer, R.: Detection of iodine monoxide
841 in the tropical free troposphere, *Proc. Nat. Acad. Sci.*, 110, 6, 2035-2040
842
843 Edwards, P., Evans, M.J., Commane, R., Ingham, T., Stone, D., Mahajan, A.S., Oetjen, H., Dorsey, J.R., Hopkins,
844 J.R., Lee, J.D., Moller, S.J., Leigh, R., Plane, J.M.C., Carpenter, L.J., Heard, D.E.: Hydrogen oxide
845 photochemistry in the northern Canadian spring time boundary layer, *J. Geophys. Res.*, 116, D22306.
846 Doi:10.1029/2011JD016390, 2011
847
848 Ehhalt, D.H., Rohrer, F.: The tropospheric cycle of H₂: a critical review, *Tellus*, 61B, 500-535, 2009
849
850 Emmerson, K.M., Evans, M.J.: Comparison of tropospheric gas-phase chemistry schemes for use within global
851 models, *Atmos. Chem. Phys.*, 9, 1831-1845, 2009
852
853 Evans, M. J., Jacob, D. J.: Impact of new laboratory studies of N₂O₅ hydrolysis on global model budgets of
854 tropospheric nitrogen oxides, ozone, and OH, *Geophys. Res. Lett.*, 32, 1–4, 2005
855
856 Fairlie, T.D., Jacob, D.J., and Park, R.J.: The impact of transpacific transport of mineral dust in the United States,
857 *Atmos. Environ.*, 41, 6, 1251-1266, doi:10.1016/j.atmosenv.2006.09.048, 2007
858
859 Fischer, E.V., Jacob, D.J., Millet, D.B., Yantosca, R.M., and Mao, J.: The role of the ocean in the global
860 atmospheric budget of acetone, *Geophys. Res. Lett.*, 39, L01807, doi:10.1029/2011gl050086, 2012
861

862 Fittschen, C., Whalley, L.K., and Heard, D.E.: The reaction of CH₃O₂ radicals with OH radicals: A neglected sink
863 for CH₃O₂ in the remote atmosphere, *Environ. Sci. Technol.*, 118, 7700-7701, 2014
864

865 Fomba, K.W., Muller, K., van Pinxteren, D., Poulain, L., van Pinxteren, M., and Herrmann, H., Long-term
866 chemical characterization of tropical and marine aerosols at the Cape Verde Atmospheric Observatory (CVAO)
867 from 2007 to 2011, *Atmos. Chem. Phys.*, 14, 17, 8883-8904, doi:10.5194/acp-14-8883-2014, 2014
868

869 Fu, T.-M., Jacob, D.J., Wittrock, F., Burrows, J.P., Vrekoussis, M., and Henze, D.K.: Global budgets of
870 atmospheric glyoxal and methylglyoxal, and implications for formation of secondary organic aerosols, *J.*
871 *Geophys. Res.*, 113, D15303, doi:10.1029/2007jd009505, 2008
872

873 Fuchs, H., Bohn, B., Hofzumahaus, A., Holland, F., Lu, K. D., Nehr, S., Rohrer, F., Wahner, A.: Detection of
874 HO₂ by laser induced fluorescence: calibration and interferences from RO₂ radicals, *Atmos. Meas. Tech.*, 4, 1209–
875 1225, 2011
876

877 George, I.J., Matthews, P.S.J., Whalley, L.K., Brooks, B., Goddard, A., Baeza-Romero, M.T., Heard, D.E.:
878 Measurements of uptake coefficients for heterogeneous loss of HO₂ onto submicron inorganic salt aerosols, *Phys.*
879 *Chem. Chem. Phys.*, 15, 12829-12845, 2013
880

881 Gomez Martin, J.C., Mahajan, A.S., Hay, T.D., Prados-Roman, C., Ordonez, C., MacDonald, S.M., Plane, J.M.C.,
882 Sorribas, M., Gil, M., Francisco Paredes Mora, J., Agama Reyes, M.V., Oram, D.E., Leedham, E., Saiz-Lopez,
883 A.: Iodine chemistry in the eastern Pacific marine boundary layer, *J. Geophys. Res. Atmos.*, 118, 887-904, 2013
884

885 Guenther, A., Karl, T., Harley, P., Wiedinmyer, C., Palmer, P.I., and Geron, C.: Estimates of global terrestrial
886 isoprene emissions using MEGAN (Model of Emissions of Gases and Aerosols from Nature), *Atmos. Chem.*
887 *Phys.*, 6, 3181-3210, 2006
888

889 Heald, C.L., Coe, H., Jimenez, J.L., Weber, R.J., Bahreini, R., Middlebrook, A.M., Russell, L.M., Jolleys, M.,
890 Fu, T.M., Allan, J.D., Bower, K.N., Capes, G., Crosier, J., Morgan, W.T., Robinson, N.H., Williams, P.I.,
891 Cubison, M.J., De Carlo, P.F., and Dunlea, E.J.: Exploring the vertical profile of atmospheric organic aerosol:
892 comparing 17 aircraft field campaigns with a global model, *Atmos. Chem. Phys.*, 11, 24, 12673-12696,
893 doi:10.5194/acp-11-12673-2011, 2011
894

895 Heard, D. E., Read, K. A., Methven, J., Al-Haider, S., Bloss, W. J., Johnson, G. P., Pilling, M. J., Seakins, P. W.,
896 Smith, S. C., Sommariva, R., Stanton, J. C., Still, T. J., Ingham, T., Brooks, B., De Leeuw, G., Jackson, A. V.,
897 McQuaid, J. B., Morgan, R., Smith, M. H., Carpenter, L. J., Carslaw, N., Hamilton, J., Hopkins, J. R., Lee, J. D.,
898 Lewis, A. C., Purvis, R. M., Wevill, D. J., Brough, N., Green, T., Mills, G., Penkett, S. A., Plane, J. M. C., Saiz-
899 Lopez, A., Worton, D., Monks, P. S., Fleming, Z., Rickard, A. R., Alfarra, M. R., Allan, J. D., Bower, K., Coe,
900 H., Cubison, M., Flynn, M., McFiggans, G., Gallagher, M., Norton, E. G., O'Dowd, C. D., Shillito, J., Topping,
901 D., Vaughan, G., Williams, P., Bitter, M., Ball, S. M., Jones, R. L., Povey, I. M., O'Doherty, S., Simmonds, P.
902 G., Allen, A., Kinnersley, R. P., Beddows, D. C. S., Dall'Osto, M., Harrison, R. M., Donovan, R. J., Heal, M. R.,
903 Jennings, S. G., Noone, C., Spain, G.: The North Atlantic Marine Boundary Layer Experiment (NAMBLEX).

904 Overview of the campaign held at Mace Head, Ireland, in summer 2002, *Atmos. Chem. Phys.*, 6, 2241–2272,
905 doi:10.5194/acp-6-2241-2006, 2006
906
907 Henze, D.K., Hakami, A., and Seinfeld, J.H.: Development of the adjoint of GEOS-Chem, *Atmos. Chem. Phys.*,
908 7, 9, 2413–2433, 2007
909
910 Henze, D.K., Seinfeld, J.H., and Shindell, D.T.: Inverse modeling and mapping US air quality influences of
911 inorganic PM_{2.5} precursor emissions using the adjoint of GEOS-Chem, *Atmos. Chem. Phys.*, 9, 16, 5877–5903,
912 2009
913
914 Hoffmann, T., O’Dowd, C.D., and Seinfeld, J.H.: Iodine oxide homogeneous nucleation: An explanation for
915 coastal new particle production, *Geophys. Res. Lett.*, 28, 10, 1949–1952, doi:10.1029/2000GL012399, 2001
916
917 Holmes, C.D., Jacob, D.J., and Yang, X.: Global lifetime of elemental mercury against oxidation by atomic
918 bromine in the free troposphere, *Geophys. Res. Lett.*, 33, L20808, doi:10.1029/2006gl027176, 2006
919
920 Holmes, C.D., Jacob, D.J., Corbitt, E.S., Mao, J., Yang, X., Talbot, R., and Slemr, F.: Global atmospheric model
921 for mercury including oxidation by bromine atoms, *Atmos. Chem. Phys.*, 10, 12037–12057, doi:10.5194/acp-10-
922 12037-2010, 2010
923
924 Hu, L., Jacob, D.J., Liu, X., Zhang, Y., Zhang, L., Kim, P.S., Sulprizio, M.P., and Yantosca, R.M.: Global budget
925 of tropospheric ozone: Evaluating recent model advances with satellite (OMI), aircraft (IAGOS), and ozonesonde
926 observations, *Atmos. Environ.*, doi:10.1016/j.atmosenv.2017.08.036, 2017
927
928 Jacob, D.J.: Heterogeneous chemistry and tropospheric ozone, *Atmos. Environ.*, 34, 2131–2159,
929 doi:10.1016/S1352-2310(99)00462-8, 2000
930
931 Jacobson, M.Z. and Turco, R.P.: SMVGEAR: A sparse-matrix, vectorized gear code for atmospheric models,
932 *Atmos. Environ.*, 28, 273–284, 1994
933
934 Jaeglé, L., Quinn, P.K., Bates, T.S., Alexander, B., and Lin, J.-T.: Global distribution of sea salt aerosols: new
935 constraints from in situ and remote sensing observations, *Atmos. Chem. Phys.*, 11, 3137–3157, doi:10.5194/acp-
936 11-3137-2011, 2011
937
938 Jenkin, M.E., Saunders, S.M., Wagner, V., Pilling, M.J., Protocol for the development of the Master Chemical
939 Mechanism, MCM v3 (Part B): tropospheric degradation of aromatic volatile organic compounds, *Atmos. Chem.*
940 *Phys.*, 3, 181–193, 2003
941
942 Kanaya, Y., Matsumoto, J., Kato, S., and Akimoto, H.: Behavior of OH and HO₂ radicals during the Observations
943 at a Remote Island of Okinawa (ORION99) field campaign. 2. Comparison between observations and
944 calculations, *J. Geophys. Res.-Atmos.*, 106, 24209–24223, 2001
945

946 Kanaya, Y., Yokouchi, Y., Matsumoto, J., Nakamura, K., Kato, S., Tanimoto, H., Furutani, H., Toyota, K., and
947 Akimoto, H.: Implications of iodine chemistry for daytime HO₂ levels at Rishiri Island, *Geophys. Res. Lett.*, 29,
948 1212, doi:10.1029/2001GL014061, 2002
949
950 Kanaya, Y., Cao, R., Kato, S., Miyakawa, Y., Kajii, Y., Tanimoto, H., Yokouchi, Y., Mochida, M., Kawamura,
951 K., Akimoto, H.: Chemistry of OH and HO₂ radicals observed at Rishiri Island, Japan, in September 2003:
952 Missing daytime sink of HO₂ and positive nighttime correlations with monoterpenes, *J. Geophys. Res.-Atmos.*,
953 112, D11308, doi:10.1029/2006JD007987, 2007
954
955 Lakey, P.S.J., George, I.J., Whalley, L.K., Baeza-Romero, M.T., and Heard, D.E.: Measurements of HO₂ uptake
956 coefficients onto single component organic aerosols, *Environ. Sci. Technol.*, 49, 8, 4878-4885,
957 doi:10.1021/acs.est.5b00948, 2015
958
959 Lee, J.D., Moller, S.J., Read, K.A., Lewis, A.C., Mendes, L., Carpenter, L.J.: Year-round measurements of
960 nitrogen oxides and ozone in the tropical North Atlantic marine boundary layer, *J. Geophys. Res.*, 114, D21302,
961 doi:10.1029/2009JD011878, 2009
962
963 Lee, J. D., McFiggans, G., Allan, J. D., Baker, A. R., Ball, S. M., Benton, A. K., Carpenter, L. J., Commane, R.,
964 Finley, B. D., Evans, M., Fuentes, E., Furneaux, K., Goddard, A., Good, N., Hamilton, J. F., Heard, D. E.,
965 Herrmann, H., Hollingsworth, A., Hopkins, J. R., Ingham, T., Irwin, M., Jones, C. E., Jones, R. L., Keene, W. C.,
966 Lawler, M. J., Lehmann, S., Lewis, A. C., Long, M. S., Mahajan, A., Methven, J., Moller, S. J., Miller, K., Muller,
967 T., Niedermeier, N., O'Doherty, S., Oetjen, H., Plane, J. M. C., Pszenny, A. A. P., Read, K. A., Saiz-Lopez, A.,
968 Saltzman, E. S., Sander, R., von Glasow, R., Whalley, L., Wiedensohler, A., Young, D.: Reactive Halogens in
969 the Marine Boundary Layer (RHaMBLe): the tropical North Atlantic experiments, *Atmos. Chem. Phys.*, 10,
970 1031–1055, 2010
971
972 [Le Breton, M., Bannan, T.J., Shallcross, D.E., Khan, A.M., Evans, M.J., Lee, J., Lidster, R., Andrews, S.,](#)
973 [Carpenter, L.J., Schmidt, J., Jacob, D., Harris, N.R.P., Bauguitte, S., Gallagher, M., Bacak, A., Leather, K.E., and](#)
974 [Percival, C.J.: Enhanced ozone loss by active inorganic bromine chemistry in the tropical troposphere. *Atmos.*](#)
975 [Environ.](#), 155, 21-28, doi:10.1016/j.atmosenv.2017.02.003, 2017
976
977 Leser, H., Honninger, G., Platt, U.: MAX-DOAS measurements of BrO and NO₂ in the marine boundary layer,
978 *Geophys. Res. Lett.*, 30, doi:10.1029/2002GL015 811, 2003
979
980 Liao, H., Henze, D.K., Seinfeld, J.H., Wu, S.L., and Mickley, L.J.: Biogenic secondary organic aerosol over the
981 United States: Comparison of climatological simulations with observations, *J. Geophys. Res. Atmos.*, 112, D6,
982 D06201, 1-19, doi:10.1029/2006JD007813, 2007
983
984 Liu, H., Jacob, D.J., Bey, I., and Yantosca, R.M.: Constraints from ²¹⁰Pb and ⁷Be on wet deposition and transport
985 in a global three-dimensional chemical tracer model driven by assimilated meteorological fields, *J. Geophys.*
986 *Res.*, 106, 12109–12128, doi:10.1029/2000jd900839, 2001
987

988 MacDonald, S.M., Gómez Martín, J.C., Chance, R., Warriner, S., Saiz-Lopez, A., Carpenter, L.J., and Plane,
989 J.M.C.: A laboratory characterisation of inorganic iodine emissions from the sea surface: dependence on oceanic
990 variables and parameterisation for global modelling, *Atmos. Chem. Phys.*, 14, 5841–5852, doi:10.5194/acp-14-
991 5841-2014, 2014

992

993 Mahajan, A.S., Plane, J.M.C., Oetjen, H., Mendes, L., Saunders, R.W., Saiz-Lopez, A., Jones, C.E., Carpenter,
994 L.J., McFiggans, G.B.: Measurement and modelling of tropospheric reactive halogen species over the tropical
995 Atlantic Ocean, *Atmos. Chem. Phys.*, 10, 4611–4624, 2010a

996

997 Mahajan, A.S., Whalley, L.K., Kozlova, E., Oetjen, H., Mendez, L., Furneaux, K.L., Goddard, A., Heard, D.E.,
998 Plane, J.M.C., Saiz-Lopez, A.: DOAS observations of formaldehyde and its impact on the HO_x balance in the
999 tropical Atlantic marine boundary layer, *J. Atmos. Chem.*, 66, 167–178, 2010b

000

001 Mahajan, A. S., Sorribas, M., Gomez Martn, J. C., MacDonald, S. M., Gil, M., Plane, J. M. C., Saiz-Lopez, A.:
002 Concurrent observations of atomic iodine, molecular iodine and ultrafine particles in a coastal environment,
003 *Atmos. Chem. Phys.*, 11, 2545–2555, doi:10.5194/acp-11-2545-2011, 2011

004

005 Mao, J., Jacob, D.J., Evans, M.J., Olson, J.R., Ren, X., Brune, W.H., Clair, J.M. St., Crounse, J.D., Spencer, K.M.,
006 Beaver, M.R., Wennberg, P.O., Cubison, M.J., Jimenez, J.L., Fried, A., Weibring, P., Walega, J.G., Hall, S.R.,
007 Weinheimer, A.J., Cohen, R.C., Chen, G., Crawford, J.H., McNaughton, C., Clarke, A.D., Jaegle, L., Fisher, J.A.,
008 Yantosca, R.M., Le Sager, P., and Carouge, C.: Chemistry of hydrogen oxide radicals (HO_x) in the Arctic
009 troposphere in spring, *Atmos. Chem. Phys.*, 10, 5823–5838, doi:10.5194/acp-10-5823-2010, 2010

010

011 Mao, J., Fan, S., Jacob, D.J., Travis, K.R.: Radical loss in the atmosphere from Cu-Fe redox coupling in aerosols,
012 *Atmos. Chem. Phys.*, 13, 509–519, 2013

013

014 Matthews, P.S.J., Baeza-Romero, M.T., Whalley, L.K., and Heard, D.E.: Uptake of HO₂ radicals onto Arizona
015 test dust particles using an aerosol flow tube, *Atmos. Chem. Phys.*, 14, 7397–7408, doi:10.5194/acp-14-7397-
016 2014, 2014

017

018 McFiggans, G., Coe, H., Burgess, R., Allan, J., Cubison, M., Alfarra, M. R., Saunders, R., Saiz-Lopez, A., Plane,
019 J. M. C., Wevill, D., Carpenter, L., Rickard, A. R., Monks, P. S.: Direct evidence for coastal iodine particles from
020 *Laminaria* macroalgae – linkage to emissions of molecular iodine, *Atmos. Chem. Phys.*, 4, 701–713,
021 doi:10.5194/acp-4-701-2004, 2004

022

023 McFiggans, G., Bale, C. S. E., Ball, S. M., Beames, J. M., Bloss, W.J., Carpenter, L. J., Dorsey, J., Dunk, R.,
024 Flynn, M. J., Furneaux, K. L., Gallagher, M. W., Heard, D. E., Hollingsworth, A. M., Hornsby, K., Ingham, T.,
025 Jones, C. E., Jones, R. L., Kramer, L. J., Langridge, J. M., Leblanc, C., LeCrane, J.-P., Lee, J. D., Leigh, R. J.,
026 Longley, I., Mahajan, A. S., Monks, P. S., Oetjen, H., Orr-Ewing, A. J., Plane, J. M. C., Potin, P., Shillings, A. J.
027 L., Thomas, F., von Glasow, R., Wada, R., Whalley, L. K., Whitehead, J. D.: Iodine-mediated coastal particle
028 formation: an overview of the Reactive Halogens in the Marine Boundary Layer (RHAMBLe) Roscoff coastal
029 study, *Atmos. Chem. Phys.*, 10, 2975–2999, doi:10.5194/acp-10-2975-2010, 2010

030

031 McLinden, C.A., Olsen, S.C., Hannegan, B., Wild, O., Prather, M.J., and Sundet, J.: Stratospheric ozone in 3-D
032 models: A simple chemistry and the cross-tropopause flux, *J. Geophys. Res.*, 105, 14653–14665, 2000
033
034 Millet, D.B., Bassandorj, M., Farmer, D.K., Thornton, J.A., Baumann, K., Brophy, P., Chaliyakunnel, S., de
035 Gouw, J.A., Graus, M., Hu, L., Koss, A., Lee, B.H., Lopez-Hilfiker, F.D., Neuman, J.A., Paulot, F., Peischl, J.,
036 Pollack, I.B., Ryerson, T.B., Warneke, C., Williams, B.J., and Xu, J.: A large and ubiquitous source of
037 atmospheric formic acid, *Atmos. Chem. Phys.*, 15, 6283-6304, doi:10.5194/acp-15-6283-2015, 2015
038
039 Muller, K., Lehmann, S., van Pinxteren, D., Gnauk, T., Niedermeier, N., Wiedensohler, A., Herrmann, H.: Particle
040 characterization at the Cape Verde atmospheric observatory during the 2007 RHaMBLe intensive, *Atmos. Chem.*
041 *Phys.*, 10, 2709-2721, 2010
042
043 Murray, L.T., Jacob, D.J., Logan, J.A., Hudman, R.C., and Koshak, W.J.: Optimized regional and interannual
044 variability of lightning in a global chemical transport model constrained by LIS/OTD satellite data, *J. Geophys.*
045 *Res. Atmos.*, 117, D20307, doi:10.1029/2012JD017934, 2012
046
047 Nassar, R., Logan, J. A., Megretskaia, I. A., Murray, L. T., Zhang, L., and Jones, D. B. A.: Analysis of tropical
048 tropospheric ozone, carbon monoxide, and water vapour during the 2006 El Nino using TES observations and the
049 GEOS-Chem model, *J. Geophys. Res.*, 114, D17304, doi:10.1029/2009JD011760, 2009
050
051 NOAA CMDL flask analysis, <ftp://ftp.cmdl.noaa.gov/ccg/ch4/>, GLOBALVIEW-CH4, 2010-2011: Cooperative
052 Atmospheric Data Integration Project – Methane. CD-ROM, NOAA ESRL, Boulder, Colorado, also available on
053 Internet via anonymous FTP to <ftp://ftp.cmdl.noaa.gov/ccg/ch4/>, path: ccg/CH4/GLOBALVIEW, 2009, access:
054 17 Feb 2010
055
056 Novelli, P.C., Lang, P.M., Masarie, K.A., Hurst, D.F., Myers, R., Elkins, J.W.: Molecular hydrogen in the
057 troposphere: Global distribution and budget, *J. Geophys. Res.*, 104, D23, 30,427-30,444, 1999
058
059 O’Dowd, C.D. and Hoffmann, T.: Coastal new particle formation: a review of the current state-of-the-art, *Environ.*
060 *Chem.*, 2, 245, doi:10.1071/EN05077, 2005
061
062 Olivier, J.G.J., and Peters, J.A.H.W.: CO₂ from non-energy use of fuels: A global, regional and national
063 perspective based on the IPCC Tier 1 approach, *Res. Conserv., Recycl.*, 45, 3, 210-225,
064 doi:10.1016/j.resconrec.2005.05.008, 2005
065
066 Ordonez, C., Lamarque, J.-F., Tilmes, S., Kinnison, D.E., Atlas, E.L., Blake, D.R., Sousa Santos, G., Brasseur,
067 G., Saiz-Lopez, A.: Bromine and iodine chemistry in a global chemistry-climate model: description and
068 evaluation of very short-lived oceanic sources, *Atmos. Chem. Phys.*, 12, 1423-1447, 2012
069
070 Park, R.J., Jacob, D.J., Field, B.D., Yantosca, R.M., and Chin, M.: Natural and transboundary pollution influences
071 on sulfate-nitrate-ammonium aerosols in the United States: Implications for policy, *J. Geophys. Res. Atmos.*, 109,
072 D15204, doi:10.1029/2003JD004473, 2004
073

074 Parrella, J.P., Jacob, D.J., Liang, Q., Zhang, Y., Mickley, L.J., Miller, B., Evans, M.J., Yang, X., Pyle, J.A., Theys,
075 N., Van Roozendaal, M.: Tropospheric bromine chemistry: implications for present and pre-industrial ozone and
076 mercury, *Atmos. Chem. Phys.*, 12, 6723-6740, 2012
077
078 Paulot, F., Crounse, J.D., Kjaergaard, H.G., Kürten, A., St. Clair, J.M., Seinfeld, J.H., and Wennberg, P.O.:
079 Unexpected Epoxide Formation in the Gas-Phase Photooxidation of Isoprene, *Science*, 325, 730-733, 2009
080
081 Peters, C., Pechtl, S., Stutz, J., Hebestreit, K., Honninger, G., Heumann, K. G., Schwarz, A., Winterlik, J., and
082 Platt, U.: Reactive and organic halogen species in three different European coastal environments, *Atmos. Chem.*
083 *Phys.*, 5, 3357-3375, doi:10.5194/acp-5-3357-2005, 2005
084
085 Pye, H.O.T., Liao, H., Wu, S., Mickley, L.J., Jacob, D.J., Henze, D.K., and Seinfeld, J.H.: Effect of changes in
086 climate and emissions on future sulfate-nitrate-ammonium aerosol levels in the United States, *J. Geophys. Res.*
087 *Atmos.*, 114, D01205, doi:10.1029/2008JD010701, 2009
088
089 Read, K. A., Mahajan, A. S., Carpenter, L. J., Evans, M. J., Faria, B. V. E., Heard, D. E., Hopkins, J. R., Lee, J.
090 D., Moller, S. J., Lewis, A. C., Mendes, L., McQuaid, J. B., Oetjen, H., Saiz-Lopez, A., Pilling, M. J., Plane, J.
091 M. C.: Extensive halogen mediated ozone destruction over the tropical Atlantic Ocean, *Nature*, 453, 7199, 1232-
092 1235, 2008
093
094 Saiz-Lopez, A. and Plane, J. M. C.: Novel iodine chemistry in the marine boundary layer, *Geophys. Res. Lett.*,
095 31, L04112, doi:10.1029/2003GL019215, 2004
096
097 Saiz-Lopez, A., Plane, J. M. C., Shillito, J. A.: Bromine oxide in the mid-latitude marine boundary layer, *Geophys.*
098 *Res. Lett.*, 31, L03111, doi:10.1029/2003GL018956, 2004
099
100 Saiz-Lopez, A., Shillito, J.A., Coe, H., Plane, J.M.C.: Measurements and modelling of I₂, IO, OIO, BrO and NO₃
101 in the mid-latitude marine boundary layer, *Atmos. Chem. Phys.*, 6, 1513-1528, 2006
102
103 Saiz-Lopez, A., Lamarque, J.-F., Kinnison, D.E., Tilmes, S., Ordóñez, C., Orlando, J.J., Conley, A.J., Plane,
104 J.M.C., Mahajan, A.S., Sousa Santos, G., Atlas, E.L., Blake, D.R., Sander, S.P., Schauffler, S., Thompson, A.M.,
105 Brasseur, G.: Estimating the climate significance of halogen-driven ozone loss in the tropical marine troposphere,
106 *Atmos. Chem. Phys.*, 12, 3939-3949, 2012
107
108 Saiz-Lopez, A., von Glasow, R.: Reactive halogen chemistry in the troposphere, *Chem. Soc. Rev.*, 41, 6448-6472,
109 2012
110
111 Sander, R., Keene, W. C., Pszenny, A. A. P., Arimoto, R., Ayers, G. P., Baboukas, E., Cainey, J. M., Crutzen, P.
112 J., Duce, R. A., Honninger, G., Huebert, B. J., Maenhaut, W., Mihalopoulos, N., Turekian, V. C., Van Dingenen,
113 R.: Inorganic bromine in the marine boundary layer: a critical review, *Atmos. Chem. Phys.*, 3, 1301-1336,
114 doi:10.5194/acp-3-1301-2003, 2003
115

116 Sander, S.P., Friedl, R.R., Abbatt, J.P.D., Barker, J.R., Burkholder, J.B., Golden, D.M., Kolb, C.E., Kurylo, M.J.,
117 Moortgat, G.K., Wine, P., Huie, R.E., and Orkin, V.L.: Chemical kinetics and photochemical data for use in
118 atmospheric studies, Evaluation Number 17, Tech. rep., NASA Jet Propulsion Laboratory, Pasadena, 2011
119
120 Sandu, A., Sander, R.: Technical note: Simulating chemical systems in Fortran90 and Matlab with the Kinetic
121 PreProcessor KPP-2.1, *Atmos. Chem. Phys.*, 6, 187-195, 2006
122
123 Saunders, S.M., Jenkin, M.E., Derwent, R.G., Pilling, M.J.: Protocol for the development of the Master Chemical
124 Mechanism, MCM v3 (Part A): tropospheric degradation of non-aromatic volatile organic compounds, *Atmos.*
125 *Chem. Phys.*, 3, 161-180, 2003
126
127 Schmidt, J.A., Jacob, D.J., Horowitz, H.M., Hu, L., Sherwen, T., Evans, M.J., Liang, Q., Suleiman, R.M., Oram,
128 D.E., Breton, M.L., Percival, C.J., Wang, S., Dix, B., and Volkamer, R.: Modeling the observed tropospheric BrO
129 background: Importance of multiphase chemistry and implications for ozone, OH, and mercury, *J. Geophys. Res.*
130 *Atmos.*, 121, 19, 11819-11835, doi:10.1002/2015JD024229, 2016
131
132 Schwarz, S. E.: Mass-transport considerations pertinent to aqueous phase reactions of gases in liquid-water
133 clouds, *Chemistry of Multiphase Atmospheric Systems*, NATO ASI Series, G6, Jaeschke ed., Springer-Verlag,
134 Berlin, 415-471, 1986
135
136 Sherwen, T., Evans, M.J., Carpenter, L.J., Andrews, S.J., Lidster, R.T., Dix, B., Koenig, T.K., Sinreich, R.,
137 Ortega, I., Volkamer, R., Saiz-Lopez, A., Prados-Roman, C., Mahajan, A. S., and Ordóñez, C.: Iodine's impact
138 on tropospheric oxidants: a global model study in GEOS-Chem, *Atmos. Chem. Phys.*, 16, 1161- 1186,
139 doi:10.5194/acp-16-1161-2016, 2016a
140
141 Sherwen, T., Schmidt, J.A., Evans, M.J., Carpenter, L.J., Großmann, K., Eastham, S.D., Jacob, D.J., Dix, B.,
142 Koenig, T.K., Sinreich, R., Ortega, I., Volkamer, R., Saiz-Lopez, A., Prados-Roman, C., Mahajan, A.S., and
143 Ordóñez, C.: Global impacts of tropospheric halogens (Cl, Br, I) on oxidants and composition in GEOS-Chem,
144 *Atmos. Chem. Phys.*, 16, 12239-12271, doi:10.5194/acp-16-12239-2016, 2016b
145
146 Sherwen, T.M., Evans, M.J., Spracklen, D.V., Carpenter, L.J., Chance, R., Baker, A.R., Schmidt, J.A., and
147 Breider, T.J.: Global modeling of tropospheric iodine aerosol, *Geophys. Res. Lett.*, 43, 18, 19912-10019,
148 doi:1002/2016GL070062, 2016c
149
150 Sherwen, T., Evans, M.J., Carpenter, L.J., Schmidt, J.A., and Mickley, L.J.: Halogen chemistry reduces
151 tropospheric O₃ radiative forcing, *Atmos. Chem. Phys.*, 17, 1557-1569, doi:10.5194/acp-17-1557-2017, 2017
152
153 Simpson, W.R., Brown, S.S., Saiz-Lopez, A., Thornton, J.A., and von Glasow, R.: Tropospheric Halogen
154 Chemistry: Sources, Cycling, and Impacts, *Chem. Rev.*, 115, 4035-4062, doi:10.1021/cr5006638, 2015
155
156 Smith, S. C., Lee, J. D., Bloss, W. J., Johnson, G. P., Ingham, T., Heard, D. E.: Concentrations of OH and HO₂
157 radicals during NAMBLEX: measurements and steady state analysis, *Atmos. Chem. Phys.*, 6, 1435-1453, 2006
158

159 Sommariva, R., Bloss, W.J., Brough, N., Carslaw, N., Flynn, M., Haggerstone, A.-L., Heard, D.E., Hopkins, J.R.,
160 Lee, J.D., Lewis, A.C., McFiggans, G., Monks, P.S., Penkett, S.A., Pilling, M.J., Plane, J.M.C., Read, K.A., Saiz-
161 Lopez, A., Rickard, A.R., Williams, P.I.: OH and HO₂ chemistry during NAMBLEX: role of oxygenates, halogen
162 oxides and heterogeneous uptake, *Atmos. Chem. Phys.*, 6, 1135-1153, 2006
163
164 Sommariva, R., Pilling, M.J., Bloss, W.J., Heard, D.E., Lee, J.D., Fleming, Z.L., Monks, P.S., Plane, J.M.C.,
165 Saiz-Lopez, A., Ball, S.M., Bitter, M., Jones, R.L., Brough, N., Penkett, S.A., Hopkins, J.R., Lewis, A.C., Read,
166 K.A.: Night-time radical chemistry during the NAMBLEX campaign, *Atmos. Chem. Phys.*, 7, 587-598, 2007
167
168 Stone, D., Evans, M.J., Commane, R., Ingham, T., Floquet, C.F.A., McQuaid, J.B., Brookes, D.M., Monks, P.S.,
169 Purvis, R., Hamilton, J.F., Hopkins, J., Lee, J., Lewis, A.C., Stewart, D., Murphy, J.G., Mills, G., Oram, D.,
170 Reeves, C.E., Heard, D.E.: HO_x observations over West Africa during AMMA: Impact of isoprene and NO_x,
171 *Atmos. Chem. Phys.*, 10, 9415-9429, 2010
172
173 Stone, D., Evans, M.J., Edwards, P.M., Commane, R., Ingham, T., Rickard, A.R., Brookes, D.M., Hopkins, J.,
174 Leigh, R.J., Lewis, A.C., Monks, A.C., Monks, P.S., Oram, D., Reeves, C.E., Stewart, D., Heard, D.E.: Isoprene
175 oxidation mechanisms: measurements and modelling of OH and HO₂ over a South-East Asian tropical rainforest
176 during the OP3 field campaign, *Atmos. Chem. Phys.*, 11, 6749-6771, 2011
177
178 Stone, D., Whalley, L.K., Heard, D.E.: Tropospheric OH and HO₂ radicals: Field measurements and model
179 comparisons, *Chem. Soc. Rev.*, 41, 6348-6404, 2012
180
181 Stone, D., Evans, M.J., Walker, H., Ingham, T., Vaughan, S., Ouyang, B., Kennedy, O.J., McLeod, M.W., Jones,
182 R.L., Hopkins, J., Punjabi, S., Lidster, R., Hamilton, J.F., Lee, J.D., Lewis, A.C., Carpenter, L.J., Forster, G.,
183 Oram, D.E., Reeves, C.E., Bauguitte, S., Morgan, W., Coe, H., Aruffo, E., Dari-Salisburgo, C., Giammaria, F.,
184 Di Carlo, P., and Heard, D.E.: Radical Chemistry at Night: Comparisons between observed and modeled HO_x,
185 NO₃ and N₂O₅ during the RONOCO project, *Atmos. Chem. Phys.*, 14, 1299-1321, 2014, doi:10.5194/acp-14-
186 1299-2014
187
188 Taketani, F., Kanaya, Y., Akimoto, H.: Kinetics of heterogeneous reactions of HO₂ radical at ambient
189 concentration levels with (NH₄)₂SO₄ and NaCl aerosol particles, *J. Phys. Chem. A.*, 112, 11, 2370-2377, 2008
190
191 Theys, N., Van Roozendaal, M., Hendrick, F., Yang, X., De Smedt, I., Richter, A., Begoin, M., Errera, Q.,
192 Johnston, P.V., Kreher, K., and De Mazière, M.: Global observations of tropospheric BrO columns using GOME-
193 2 satellite data, *Atmos. Chem. Phys.*, 11, 1791-1811, doi:10.5194/acp-11-1791-2011, 2011
194
195 Thornton, J.A., Jaegle, L., and McNeill, V.F.: Assessing known pathways for HO₂ loss in aqueous atmospheric
196 aerosols: Regional and global impacts on tropospheric oxidants, *J. Geophys. Res. Atmos.*, 113, D5, D05303, 1-
197 16, doi:10.1029/2007JD009236, 2008
198
199 van het Bolscher, M., REanalysis of the TROpospheric chemical composition over the past 40 years: A long-term
200 global modeling study of tropospheric chemistry funded under the 5th EU framework programme, *Rep. EU-*
201 *Contract No. EVK2-CT-2002-00170*, 1-77, MPI for Meteorology, Hamburg, Germany

202
203
204
205
206
207
208
209
210
211
212
213
214
215
216
217
218
219
220
221
222
223
224
225
226
227
228
229
230
231
232
233
234
235
236
237
238
239
240
241
242
243
244

Vaughan, S., Ingham, T., Whalley, L.K., Stone, D., Evans, M.J., Read, K.A., Lee, J.D., Moller, S.J., Carpenter, L.J., Lewis, A.C., Fleming, Z.L., Heard, D.E.: Seasonal observations of OH and HO₂ in the remote tropical marine boundary layer, *Atmos. Chem. Phys.*, 12, 2149–2172, 2012

Vogt, R., Crutzen, P., and Sander, R.: A mechanism for halogen release from sea-salt aerosol in the remote marine boundary layer, *Nature*, 383, 327–330, 1996

Vogt, R., Sander, R., von Glasow, R., and Crutzen, P. J.: Iodine chemistry and its role in halogen activation and ozone loss in the marine boundary layer: A model study, *J. Atmos. Chem.*, 32, 375–395, 1999

Volkamer, R., Baidar, S., Campos, T.L., Coburn, S., DiGangi, J.P., Dix, B., Eloranta, E.W., Koenig, T.K., Morley, B., Ortega, I., Pierce, B.R., Reeves, M., Sinreich, R., Wang, S., Zondlo, M.A., and Romashkin, P.A.: Aircraft measurements of BrO, IO, glyoxal, NO₂, H₂O, O₂-O₂ and aerosol extinction profiles in the tropics: comparison with aircraft-/ship-based in situ and lidar measurements, *Atmos. Meas. Tech.*, 8, 2121–2148, doi:10.5194/amt-8-2121-2015, 2015

von Glasow, R., von Kuhlmann, R., Lawrence, M. G., Platt, U., Crutzen, P. J.: Impact of reactive bromine chemistry in the troposphere, *Atmos. Chem. Phys.*, 4, 2481–2497, 2004

Wang, Y., Jacob, D.J., and Logan, J.A.: Global simulation of tropospheric O₃-NO_x-hydrocarbon chemistry 1. Model formulation, *J. Geophys. Res.*, 103, 10713–10725, doi:10.1029/98jd00158, 1998

Wang, Q., Jacob, D.J., Fisher, J.A., Mao, J., Leibensperger, E.M., Carouge, C.C., Le Sager, P., Kondo, Y., Jimenez, J.L., Cubison, M.J., and Doherty, S.J.: Sources of carbonaceous aerosols and deposited black carbon in the Arctic in winter-spring: implications for radiative forcing, *Atmos. Chem. Phys.*, 11, 23, 12453–12473, doi:10.5194/acp-11-12453-2011, 2011

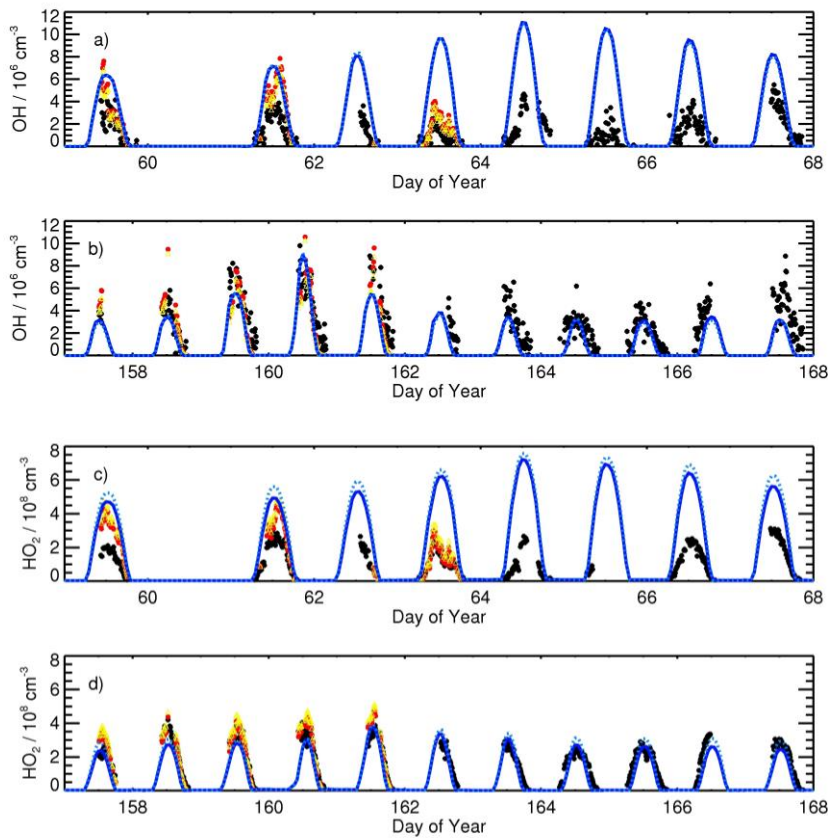
Wang, S.-Y., Schmidtd, J., Baidar, S., Coburn, S., Dix, B., Koenig, T., Apel, E., Bowdalo, D., Campos, T., Eloranta, E., Evans, M., DiGangii, J., Zondlo, M., Gao, R.-S., Haggerty, J., Hall, S., Hornbrook, R., Jacob, D., Morley, B., Pierce, B., Reeves, M., Romashkin, P., ter Schure, A., and Volkamer, R.: Active and widespread halogen chemistry in the tropical and subtropical free troposphere, *P. Natl. Acad. Sci. USA*, 112, 9281–9286, doi:10.1073/pnas.1505142112, 2015

Wesely, M.L.: Parameterization of surface resistance to gaseous dry deposition in regional-scale numerical models, *Atmos. Environ.*, 23, 1293–1304, 1989

Whalley, L. K., Furneaux, K. L., Gravestock, T., Atkinson, H. M., Bale, C. S. E., Ingham, T., Bloss, W. J., Heard, D. E.: Detection of iodine monoxide radicals in the marine boundary layer using laser induced fluorescence spectroscopy, *J. Atmos. Chem.*, 58(1), 19–39, 2007

Whalley, L.K., Furneaux, K.L., Goddard, A., Lee, J.D., Mahajan, A., Oetjen, H., Read, K.A., Kaaden, N., Carpenter, L.J., Lewis, A.C., Plane, J.M.C., Saltzman, E.S., Wiedensohler, A., Heard, D.E.: The chemistry of OH

245 and HO₂ radicals in the boundary layer over the tropical Atlantic Ocean, *Atmos. Chem. Phys.*, 10, 1555-1576,
246 2010
247
248 Whalley, L.K., Blitz, M.A., Desservettaz, M., Seakins, P.W., and Heard, D.E.: Reporting the sensitivity of laser-
249 induced fluorescence instruments used for HO₂ detection to an interference from RO₂ radicals and introducing a
250 novel approach that enables HO₂ and certain RO₂ types to be selectively measured, *Atmos. Meas. Tech.*, 6, 3425-
251 3440, 2013, doi:10.5194/amt-6-3425-2013
252
253 Wild, O., Zhu, X., and Prather, M.J.: Fast-J: Accurate Simulation of In- and Below-Cloud Photolysis in
254 Tropospheric Chemical Models, *J. Atmos. Chem.*, 37, 245–282, doi:10.1023/a:1006415919030, 2000
255
256 Yan, C., Kocevskaja, S., and Krasnoperov, L.N.: Kinetics of the reaction of CH₃O₂ radicals with OH studied over
257 the 292-526 K temperature range, *J. Phys. Chem. A*, 120, 6111-6121, 2016
258
259 Yang, X., Cox, R. A., Warwick, N. J., Pyle, J. A., Carver, G. D., O'Connor, F. M., Savage, N. H.: Tropospheric
260 bromine chemistry and its impacts on ozone: A model study, *J. Geophys. Res.*, 110, D23311,
261 doi:10.1029/2005JD006244, 2005
262
263 Zhang, L., Jacob, D.J., Liu, X., Logan, J.A., Chance, K., Eldering, A., and Bojkov, B.R.: Intercomparison methods
264 for satellite measurements of atmospheric composition: application to tropospheric ozone from TES and OMI,
265 *Atmos. Chem. Phys.*, 10, 4725–4739, doi:10.5194/acp-10-4725-2010, 2010
266



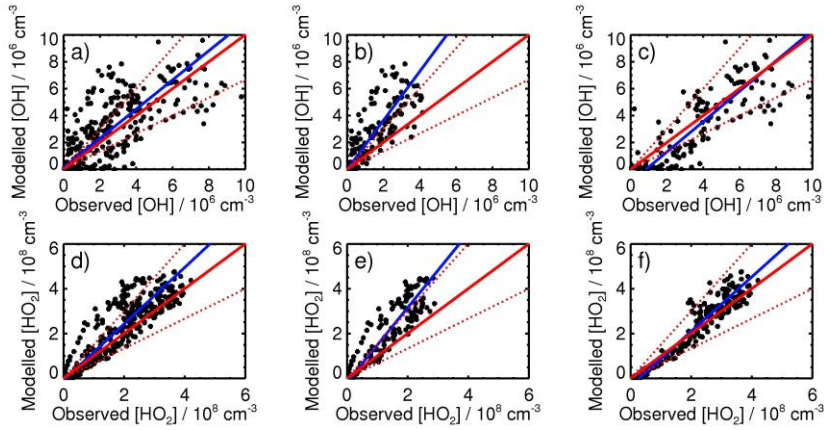
268

269

270 Figure 1: Observed and modelled concentrations of a) OH during SOS1 (February-March 2009, days 58-68); b)
 271 OH during SOS2 (May-June 2009, days 157-168); c) HO₂ during SOS1; d) HO₂ during SOS2. Observed data are
 272 shown in black; box model concentrations with halogen chemistry are shown by filled red circles; box model
 273 concentrations without halogen chemistry are shown by open yellow triangles; global model concentrations with
 274 halogen chemistry are shown by solid dark blue lines; global model concentrations without halogen chemistry
 275 are shown by broken blue lines.

276

Deleted: orange



278

279

280

281

282

283

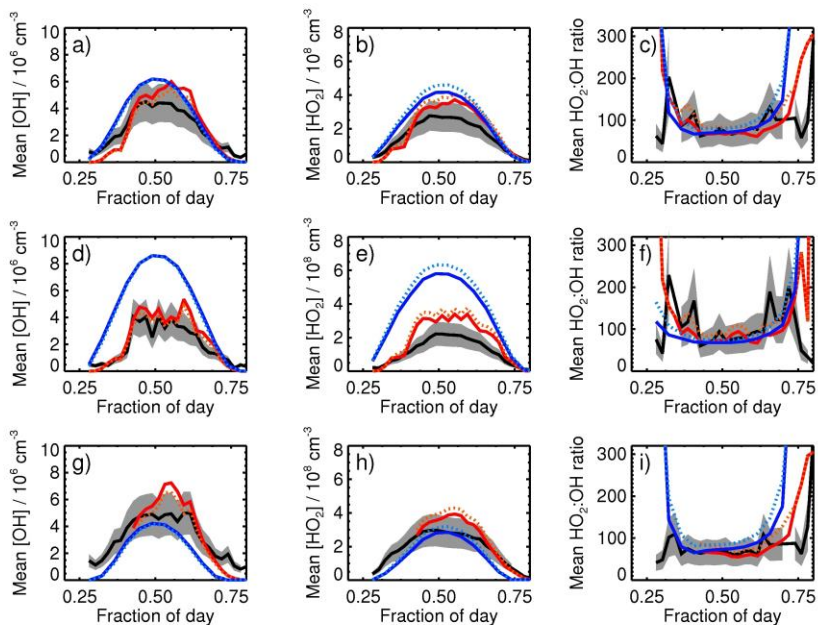
284

285

286

287

Figure 2: Comparison of modelled and observed concentrations of a) OH during SOS1 (February-March 2009) and SOS2 (May-June 2009); b) OH during SOS1; c) OH during SOS2; d) HO₂ during SOS1 and SOS2; e) HO₂ during SOS1; f) HO₂ during SOS2. In each plot, the solid red line indicates the 1:1 line, with 50 % limits given by the broken red lines. The best fit lines are shown in blue and are described by a) $[\text{OH}]_{\text{mod}} = (1.09 \pm 0.11) \times [\text{OH}]_{\text{obs}} + (0.13 \pm 0.38) \times 10^6$ ($r^2 = 0.49$); b) $[\text{OH}]_{\text{mod}} = (1.82 \pm 0.26) \times [\text{OH}]_{\text{obs}} - (0.01 \pm 0.51) \times 10^6$ ($r^2 = 0.56$); c) $[\text{OH}]_{\text{mod}} = (1.11 \pm 0.15) \times [\text{OH}]_{\text{obs}} - (0.95 \pm 0.66) \times 10^6$ ($r^2 = 0.64$); d) $[\text{HO}_2]_{\text{mod}} = (1.26 \pm 0.10) \times [\text{HO}_2]_{\text{obs}} - (0.08 \pm 0.22) \times 10^8$ ($r^2 = 0.77$); e) $[\text{HO}_2]_{\text{mod}} = (1.66 \pm 0.21) \times [\text{HO}_2]_{\text{obs}} - (0.17 \pm 0.34) \times 10^8$ ($r^2 = 0.78$); f) $[\text{HO}_2]_{\text{mod}} = (1.21 \pm 0.12) \times [\text{HO}_2]_{\text{obs}} - (0.32 \pm 0.30) \times 10^8$ ($r^2 = 0.91$).



288

289

290

291

292

293

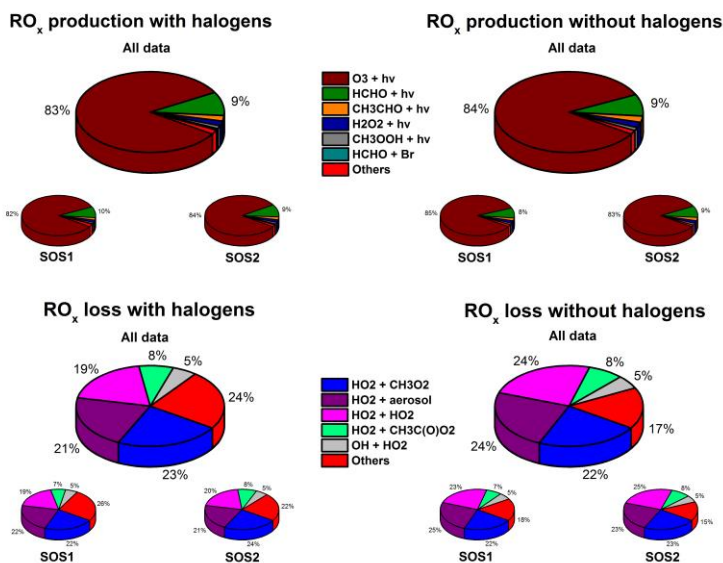
294

295

296

297

Figure 3: Average diurnal profiles during the Seasonal Oxidant Study (SOS) at the Cape Verde Atmospheric Observatory for a) OH during both measurement periods; b) HO₂ during both measurement periods; c) HO₂:OH ratio during both measurement periods; d) OH during SOS1 (Feb-Mar 2009); e) HO₂ during SOS1; f) HO₂:OH ratio during SOS1; g) OH during SOS2 (May-June); h) HO₂ during SOS2; i) HO₂:OH ratio during SOS2. Observed data are shown in black, with grey shading indicating the variability in the observations; box model output with halogen chemistry is shown by solid red lines; box model output without halogen chemistry is shown by broken orange lines; global model output with halogen chemistry is shown by solid dark blue lines; global model output without halogen chemistry is shown by broken blue lines.



298

299

300

301

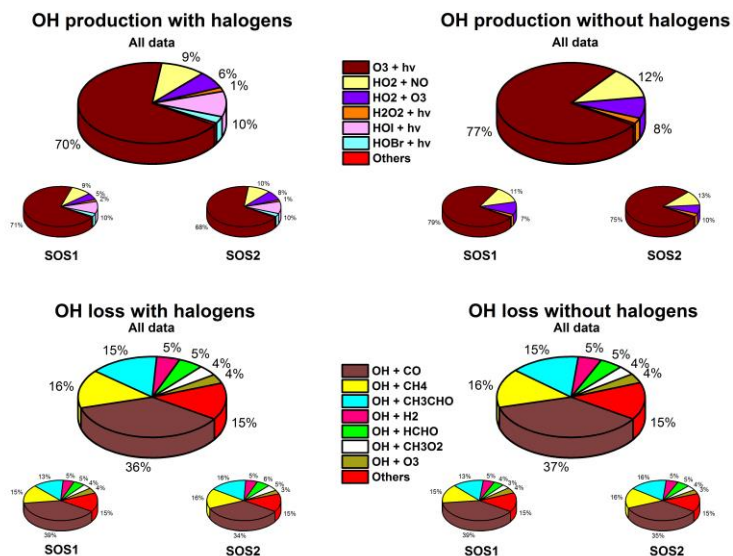
302

303

304

305

Figure 4: Processes controlling the a) instantaneous RO_x radical production (with RO_x defined here as OH+HO₂+HOBr+HOI+RO+RO₂ owing to the rapid processing between HO₂ and HOBr/HOI) around noon (1100-1300 hours) for box model simulations with halogen chemistry; b) the instantaneous RO_x radical production around noon for box model simulations without halogen chemistry; c) the instantaneous RO_x radical loss around noon for box model simulations with halogen chemistry; d) the instantaneous RO_x radical loss around noon for box model simulations without halogen chemistry. The main charts show the average results for SOS1+SOS2, with results for SOS1 and SOS2 shown separately in the inset charts.



306

307

308

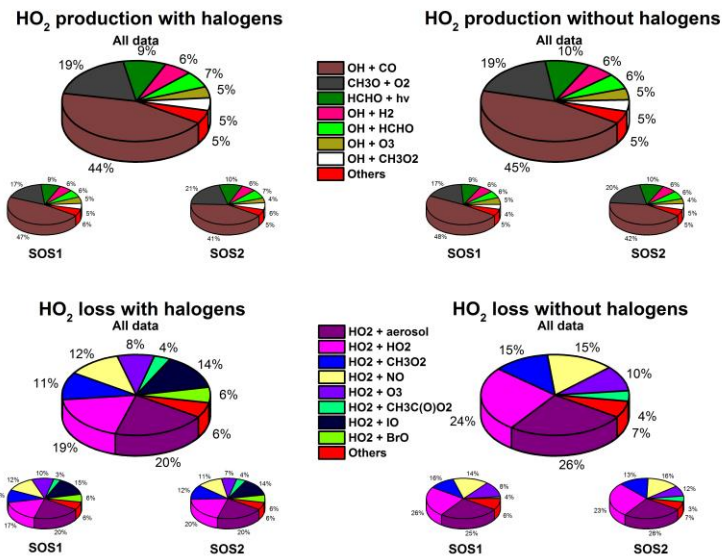
309

310

311

312

Figure 5: Processes controlling the a) instantaneous OH radical production around noon (1100-1300 hours) for box model simulations with halogen chemistry; b) the instantaneous OH radical production around noon for box model simulations without halogen chemistry; c) the instantaneous OH radical loss around noon for box model simulations with halogen chemistry; d) the instantaneous OH radical loss around noon for box model simulations without halogen chemistry. The main charts show the average results for SOS1+SOS2, with results for SOS1 and SOS2 shown separately in the inset charts.



313

314

315

316

317

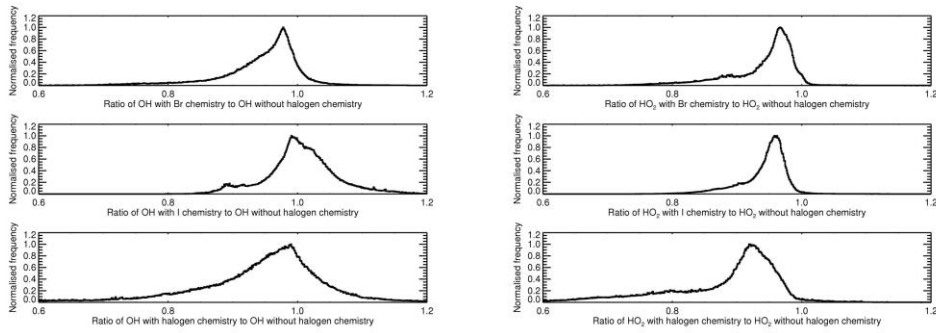
318

319

320

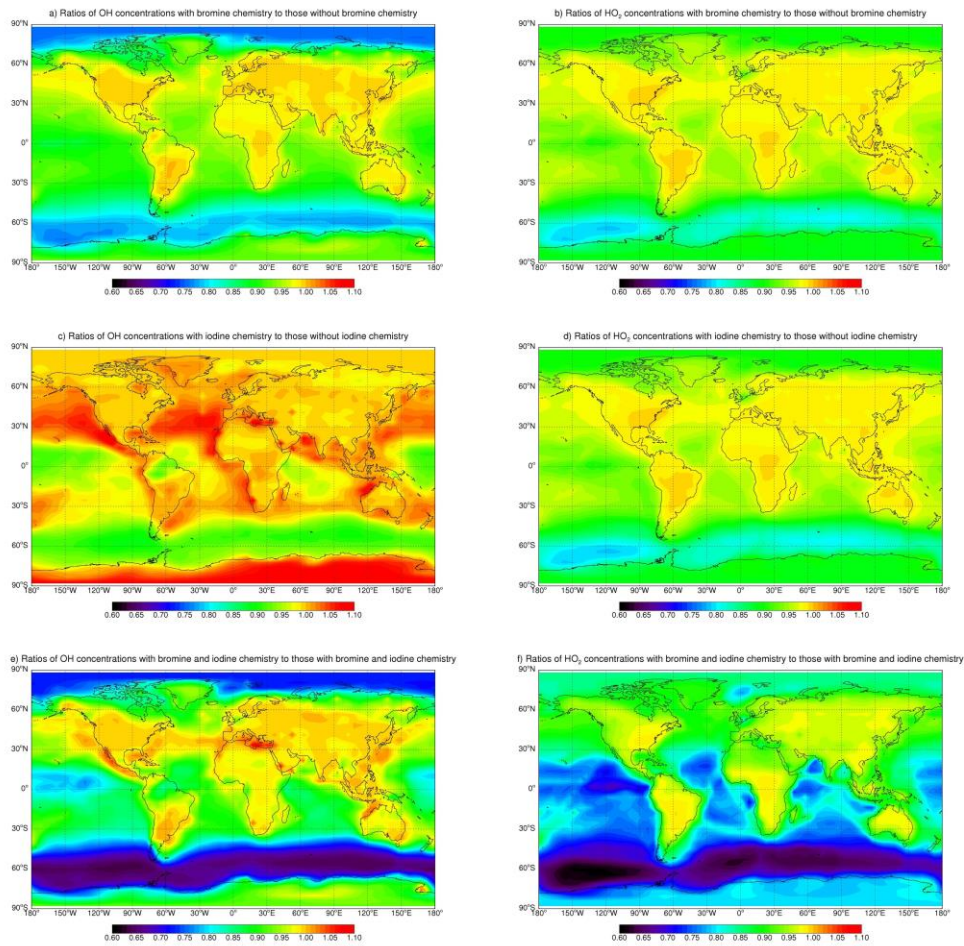
Figure 6: Processes controlling the a) instantaneous HO₂ radical production around noon (1100-1300 hours) for box model simulations with halogen chemistry; b) the instantaneous HO₂ radical production around noon for box model simulations without halogen chemistry; c) the instantaneous HO₂ radical loss around noon for box model simulations with halogen chemistry; d) the instantaneous HO₂ radical loss around noon for box model simulations without halogen chemistry. The main charts show the average results for SOS1+SOS2, with results for SOS1 and SOS2 shown separately in the inset charts.

321
322



323
324
325
326

Figure 7: Normalised probability distribution functions showing the fractional changes in OH (left hand side) and HO₂ (right hand side) in GEOS-Chem for all grid boxes on inclusion of bromine chemistry (upper panels), iodine chemistry (middle panels) and bromine and iodine chemistry combined (lower panels).



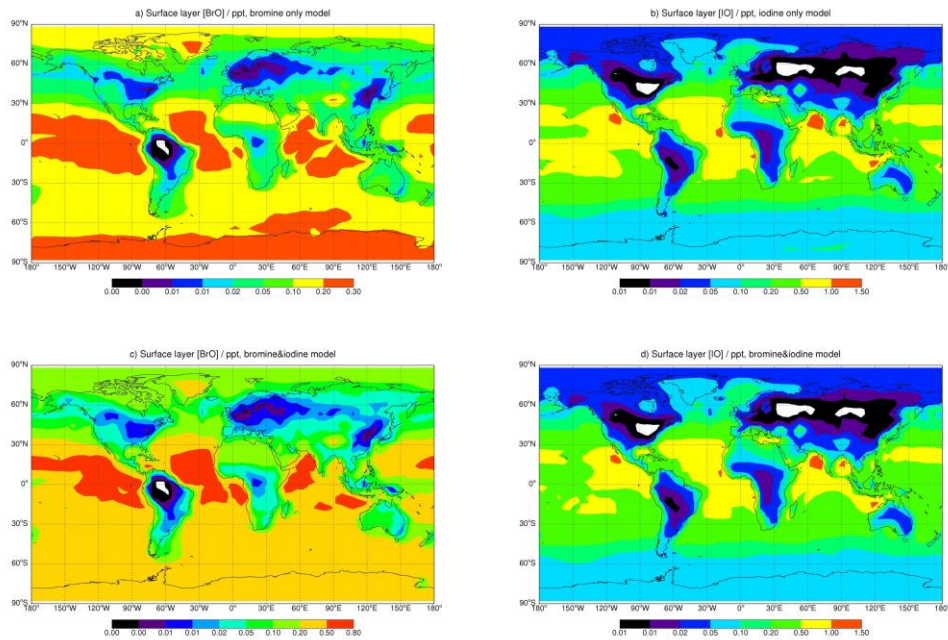
327

328

329

330

Figure 8: Percentage changes to annual surface layer concentrations of OH (left hand side) and HO₂ (right hand side) in GEOS-Chem on inclusion of bromine chemistry (upper panels), iodine chemistry (middle panels) and bromine and iodine chemistry combined (lower panels).



331
332
333
334
335
336
337

Figure 9: Annual surface layer mixing ratios (ppt) of BrO and IO radicals in GEOS-Chem for model runs with just bromine chemistry (upper left panel), just iodine chemistry (upper right panel) and bromine and iodine chemistry combined (lower panels).

Impacts of bromine and iodine chemistry on tropospheric OH and HO₂: Comparing observations with box and global model perspectives

Daniel Stone,¹ Tomás Sherwen,² Mathew J. Evans,^{2,3} Stewart Vaughan,¹ Trevor Ingham,^{1,4}
Lisa K. Whalley,^{1,4} Peter M. Edwards,² Katie A. Read,^{2,3} James D. Lee,^{2,3} Sarah J. Moller,^{2,3}
Lucy J. Carpenter,^{2,3} Alastair C. Lewis,^{2,3} Dwayne E. Heard^{1,4}

¹ School of Chemistry, University of Leeds, Leeds, UK

² Wolfson Atmospheric Chemistry Laboratories, Department of Chemistry, University of York, York, UK

³ National Centre for Atmospheric Science, University of York, York, UK

⁴ National Centre for Atmospheric Science, University of Leeds, Leeds, UK

* Now at Department of Chemistry, University of York, York, UK

Supplementary Material

Speciation of modelled peroxy radicals

Figure S1 shows the speciation of peroxy radicals during SOS determined by the box model. The dominant species at Cape Verde are HO₂ and CH₃O₂, which comprise 87.4 % of the total peroxy radical concentration, and are followed by CH₃C(O)O₂ (6.5 %) and C₂H₅O₂ (1.1 %), all of which display no HO₂ interference in the laboratory (Whalley et al., 2013; Stone et al., 2014). Any peroxy species potentially contributing to interferences in HO₂ measurements thus constitutes < 4 % of the total peroxy radical concentration, with each species representing < 1 % of the total. Potential interferences arising from conversion of alkene- and aromatic-derived peroxy radicals to OH within the LIF detection cell, as described by Fuchs et al. (2011), are thus expected to be small for SOS and are not explicitly described in the model for this work.

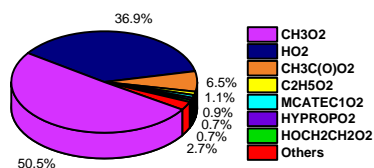


Figure S1: Speciation of peroxy radicals during SOS1 and SOS2. Radical names are as given by the MCM.

Impact of $\text{CH}_3\text{O}_2 + \text{OH}$

Recent experiments have indicated a rapid reaction between CH_3O_2 and OH (Bossolasco et al., 2014; Fittschen et al., 2014; Assaf et al., 2016; Yan et al., 2016), with the dominant products expected to be $\text{CH}_3\text{O} + \text{HO}_2$ at an observed yield of (0.8 ± 0.2) (Assaf et al., 2017). As shown in Figures 5 and 6 (main text), this reaction contributes 4 %, on average, to the total midday OH loss during SOS and 5 % to the total HO_2 production, assuming 100 % yield of $\text{CH}_3\text{O} + \text{HO}_2$. Inclusion of the reaction in the chemistry scheme, for model runs in which halogens are included, decreases the modelled concentration of OH at midday from $5.3 \times 10^6 \text{ cm}^{-3}$ to $5.2 \times 10^6 \text{ cm}^{-3}$, and increases the HO_2 concentration from $3.2 \times 10^8 \text{ cm}^{-3}$ to $3.9 \times 10^8 \text{ cm}^{-3}$.

Figure S2 shows the mean modelled diurnal profile for CH_3O_2 during SOS, for model runs with and without the reaction between CH_3O_2 and OH. Inclusion of the reaction decreases the mean midday CH_3O_2 concentration by 24 %, from $5.7 \times 10^8 \text{ cm}^{-3}$ to $4.6 \times 10^8 \text{ cm}^{-3}$, and thus has a more significant impact on CH_3O_2 than on OH or HO_2 . Similar changes to modelled OH, HO_2 and CH_3O_2 were reported by Assaf et al. (2017) using an updated MCM based model for the RHAMBLE campaign in Cape Verde in 2007 (Whalley et al., 2010).

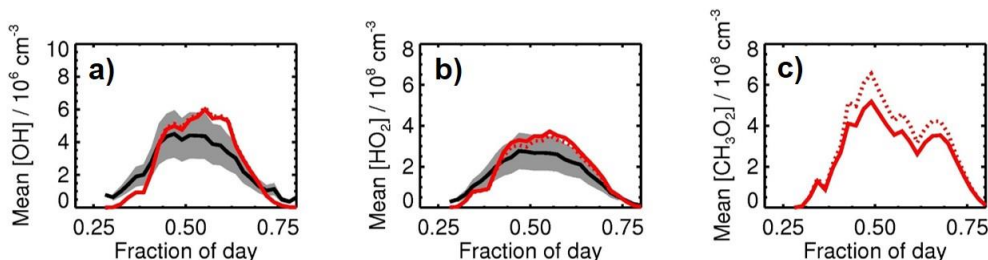
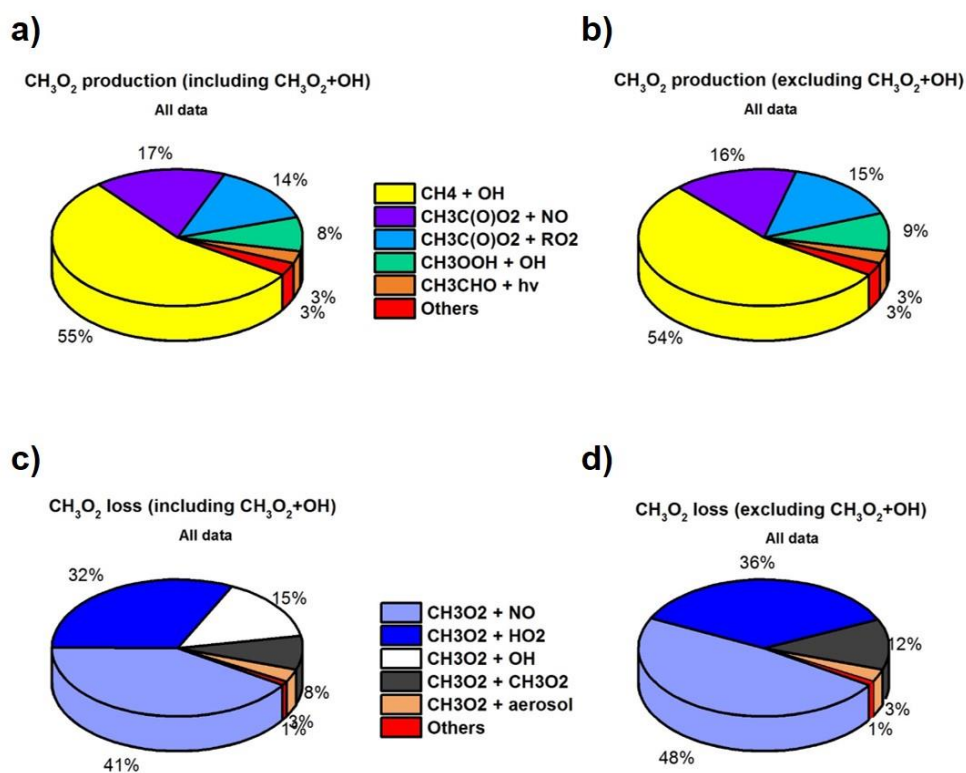


Figure S2: Mean box modelled diurnal profiles for a) OH; b) HO_2 ; c) CH_3O_2 during SOS (SOS1 and SOS2 combined) for model runs with (red solid line) and without (red broken line) the reaction between CH_3O_2 and OH. For OH and HO_2 , observations are shown in black, with grey shading indicating the variability in the observations.

Figure S3 shows the mean midday (1100 to 1300 hours) budgets for CH_3O_2 during SOS for model runs with and without the reaction between CH_3O_2 and OH. Midday production of CH_3O_2 , both with and without the reaction between CH_3O_2 and OH, is dominated by CH_3 radical production from $\text{CH}_4 + \text{OH}$ (~ 55 %), and is followed by the reactions of $\text{CH}_3\text{C}(\text{O})\text{O}_2$ radicals with NO (~ 17 %) and other RO_2 radicals (~ 15 %). Midday loss of CH_3O_2 , when CH_3O_2 is included, is dominated by reactions with NO (~ 41 %), HO_2 (~ 33 %), the reaction with OH (~ 15 %), and CH_3O_2 self-reaction (~ 8 %). If the reaction of CH_3O_2 with OH is not included in the model, the loss

392 reaction with NO represents ~ 48 % of the total CH₃O₂ loss and the reactions with HO₂ and other CH₃O₂ radicals
 393 represent ~ 36 % and ~ 12 %, respectively.

394



395

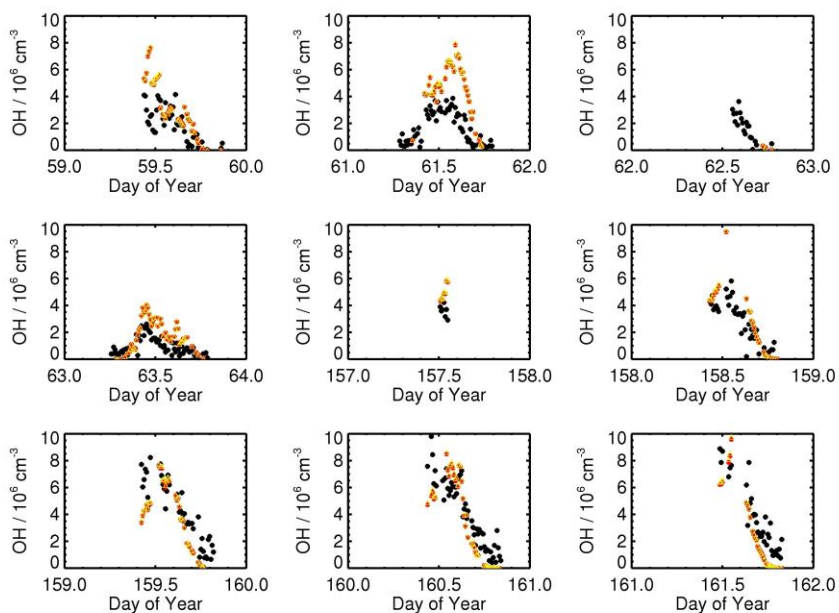
396 Figure S3: Mean midday (1100 to 1300 hours) budgets for CH₃O₂ during SOS (SOS1 and SOS2 combined). Panel
 397 a) production of CH₃O₂ for model runs with the reaction between CH₃O₂ and OH; b) production of CH₃O₂ for
 398 model runs without the reaction between CH₃O₂ and OH; c) loss of CH₃O₂ for model runs with the reaction
 399 between CH₃O₂ and OH; d) loss of CH₃O₂ for model runs without the reaction between CH₃O₂ and OH.

400

401

402 **Time series for observed and box modelled OH and HO₂ radical concentrations**

403 Figures S4 and S5 shows the times series for OH and HO₂ observations and model simulations day-by-day during
404 SOS1 and SOS2.
405



406
407 Figure S4: Times series for observed and modelled OH during SOS1 (days 59 to 63) and SOS2 (days 157 to 162).
408 Observed data are shown in black; box model concentrations with halogen chemistry are shown by filled red
409 circles; box model concentrations without halogen chemistry are shown by open yellow triangles.
410

Deleted: orange

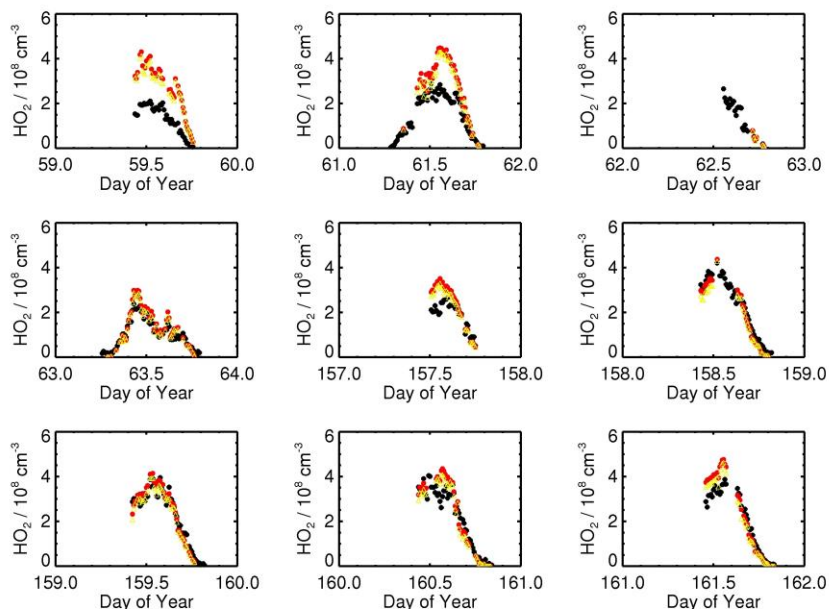


Figure S5: Times series for observed and modelled HO₂ during SOS1 (days 59 to 63) and SOS2 (days 157 to 162). Observed data are shown in black; box model concentrations with halogen chemistry are shown by filled red circles; box model concentrations without halogen chemistry are shown by open yellow triangles.

Deleted: orange

Box model sensitivity of OH and HO₂ to BrO and IO mixing ratios

Observations of BrO and IO at the Cape Verde Atmospheric Observatory show average diurnal mixing ratios of 2.5 ppt and 1.4 ppt, respectively, which were used as constraints in the box model simulations presented in this work. In order to test the sensitivity of OH and HO₂ to these constraints, we have performed simulations in which the BrO and IO mixing ratios were constrained to the upper and lower limits of the observed values (3.5 ppt and 1.5 ppt for BrO and 2.0 ppt and 1.0 ppt for IO, as reported by Read et al. (2008) and Mahajan et al. (2010)). In addition, simulations were performed in which mixing ratios of BrO and IO increase from 0600 hours and reach the constant values of 2.5 ppt and 1.4 ppt, respectively, as shown by Read et al. (2008). Results from these simulations are shown in Figure S6, and indicate that there are only minor differences in the OH and HO₂ concentrations between simulations performed on constraining to the upper and lower limits of the observed BrO

and IO concentrations, and that there is little sensitivity of OH or HO₂ to the early morning mixing ratios of BrO and IO.

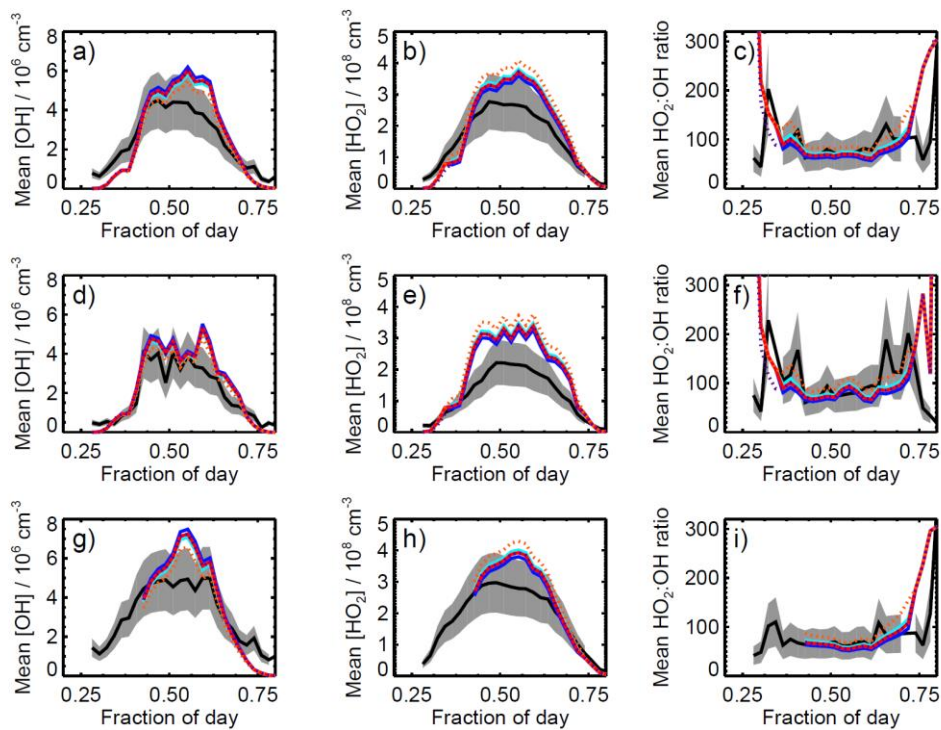


Figure S6: Impacts of changes to BrO and IO constraints on average diurnal profiles for a) OH during both measurement periods; b) HO₂ during both measurement periods; c) HO₂:OH ratio during both measurement periods; d) OH during SOS1 (Feb-Mar 2009); e) HO₂ during SOS1; f) HO₂:OH during SOS1; g) OH during SOS2 (May-June); h) HO₂ during SOS2; i) HO₂:OH ratio during SOS2. Observed data are shown in black, with grey shading indicating the variability in the observations; model simulations constrained to the average daytime (0930 to 1830 hours) mixing ratios of BrO (2.5 ppt) and IO (1.4 ppt) are shown in red; simulations constrained to the upper limits to the daytime mixing ratios of BrO (3.5 ppt) and IO (2.0 ppt) are shown in dark blue; simulations constrained to the lower limits to the daytime mixing ratios of BrO (1.5 ppt) and IO (1.0 ppt) are shown in light blue; simulations constrained to the average daytime mixing ratios of BrO (2.5 ppt) and IO (1.4 ppt) and including increases in the mixing ratios from 0600 hours are shown by the dashed purple lines; simulations with no halogens are shown by the dashed orange lines.

Deleted: ¶

References

- Assaf, E., Song, B., Tomas, A., Schoemaker, C., and Fittschen, C.: Rate constant of the reaction between CH_3O_2 and OH radicals revisited, *J. Phys. Chem. A*, 120, 8923-8932, 2016
- Assaf, E., Sheps, L., Whalley, L., Heard, D., Tomas, A., Schoemaeker, C., and Fittschen, C.: The reaction between CH_3O_2 and OH radicals: Product yields and atmospheric implications, *Environ. Sci. Technol.*, 51, 4, 2170-2177, doi: 10.1021/acs.est.6b06265, 2017
- Bossolasco, A., Farago, E.P., Schoemaker, C., and Fittschen, C.: Rate constant of the reaction between CH_3O_2 and OH radicals, *Chem. Phys. Lett.*, 593, 7-13, 2014
- Fittschen, C., Whalley, L.K., and Heard, D.E.: The reaction of CH_3O_2 radicals with OH radicals: A neglected sink for CH_3O_2 in the remote atmosphere, *Environ. Sci. Technol.*, 118, 7700-7701, 2014
- Fuchs, H., Bohn, B., Hofzumahaus, A., Holland, F., Lu, K. D., Nehr, S., Rohrer, F., Wahner, A.: Detection of HO_2 by laser induced fluorescence: calibration and interferences from RO_2 radicals, *Atmos. Meas. Tech.*, 4, 1209–1225, 2011
- [Mahajan, A.S., Plane, J.M.C., Oetjen, H., Mendes, L., Saunders, R.W., Saiz-Lopez, A., Jones, C.E., Carpenter, L.J., McFiggans, G.B.: Measurement and modelling of tropospheric reactive halogen species over the tropical Atlantic Ocean, *Atmos. Chem. Phys.*, 10, 4611-4624, 2010](#)
- [Read, K. A., Mahajan, A. S., Carpenter, L. J., Evans, M. J., Faria, B. V. E., Heard, D. E., Hopkins, J. R., Lee, J. D., Moller, S. J., Lewis, A. C., Mendes, L., McQuaid, J. B., Oetjen, H., Saiz-Lopez, A., Pilling, M. J., Plane, J. M. C.: Extensive halogen mediated ozone destruction over the tropical Atlantic Ocean, *Nature*, 453, 7199, 1232–1235, 2008](#)
- Stone, D., Evans, M.J., Walker, H., Ingham, T., Vaughan, S., Ouyang, B., Kennedy, O.J., McLeod, M.W., Jones, R.L., Hopkins, J., Punjabi, S., Lidster, R., Hamilton, J.F., Lee, J.D., Lewis, A.C., Carpenter, L.J., Forster, G., Oram, D.E., Reeves, C.E., Bauguitte, S., Morgan, W., Coe, H., Aruffo, E., Dari-Salisburgo, C., Giammaria, F., Di Carlo, P., and Heard, D.E.: Radical Chemistry at Night: Comparisons between observed and modeled HO_x , NO_3 and N_2O_5 during the RONOCO project, *Atmos. Chem. Phys.*, 14, 1299-1321, 2014, doi:10.5194/acp-14-1299-2014
- Whalley, L.K., Furneaux, K.L., Goddard, A., Lee, J.D., Mahajan, A., Oetjen, H., Read, K.A., Kaaden, N., Carpenter, L.J., Lewis, A.C., Plane, J.M.C., Saltzman, E.S., Wiedensohler, A., Heard, D.E.: The chemistry of OH and HO_2 radicals in the boundary layer over the tropical Atlantic Ocean, *Atmos. Chem. Phys.*, 10, 1555-1576, 2010
- Whalley, L.K., Blitz, M.A., Desservettaz, M., Seakins, P.W., and Heard, D.E.: Reporting the sensitivity of laser-induced fluorescence instruments used for HO_2 detection to an interference from RO_2 radicals and introducing a novel approach that enables HO_2 and certain RO_2 types to be selectively measured, *Atmos. Meas. Tech.*, 6, 3425-3440, 2013, doi:10.5194/amt-6-3425-2013

486

487 Yan, C., Kocevska, S., and Krasnoperov, L.N.: Kinetics of the reaction of CH_3O_2 radicals with OH studied over
488 the 292-526 K temperature range, J. Phys. Chem. A, 120, 6111-6121, 2016

489

490